Monofunctional dimetallic Ru(η6-arene) complexes inhibit NOTCH1 signaling pathway and synergistically enhance anticancer effect in combination with cisplatin or vitamin C

Na Wang, Amjad Ali, Zongwei Liu, Huiqin Chi, Zhimin Lv, Xing Zhao, Zeqing Zhang, Huifang Hao, Yongmin Zhang, Faiz-Ur Rahman

Monofunctional dimetallic Ru(η6-arene) complexes inhibit NOTCH1 signaling pathway and synergistically enhance anticancer effect in combination with cisplatin or vitamin C

Na Wang[a,1], Amjad Ali[b,c,1], Zongwei Liu[a,1], Huiqin Chi[a], Zhimin Lv[a], Xing Zhao[a], Zeqing Zhang[a], Huifang Hao[a,d], Yongmin Zhang[a,e,*] and Faiz-Ur Rahman[a,*]

[a]Inner Mongolia University Research Center for Glycochemistry of Characteristic Medicinal Resources, Department of Chemistry and Chemical Engineering, Inner Mongolia University, Hohhot 010021, People's Republic of China

[b]Institute of Integrative Biosciences, CECOS University of IT and Emerging Sciences, Peshawar, KPK, Pakistan.

[c]Institute of Biomedical Sciences, School of Life Sciences, East China Normal University, 500 Dongchuan Road, Shanghai, 200241, People's Republic of China.

[d]School of Life Sciences, Inner Mongolia University, Hohhot 010021, People's Republic of China

[e]Sorbonne Université, CNRS, Institut Parisien de Chimie Moléculaire, UMR 8232, 4 Place Jussieu, 75005 Paris, France.

*Corresponding authors. E-mail: yongmin.zhang@upmc.fr (Y. Zhang), faiz@imu.edu.cn (F.-U. Rahman)

Abstract

ONS donor ligands **L1**-**L4** were utilized in the preparation of monofunctional dimetallic Ru(η6-arene) complexes (**C1**-**C4**). These ONS donor ligand based novel tricoordinated Ru(II) complexes bearing η6-arene co-ligand were prepared for the first time. The current methodology resulted in excellent isolated yields and these complexes were characterized in detail by different

[1] These authors have equal contribution.

spectroscopic and spectrometric techniques. The structures of **C1-C2** and **C4** were characterized in solid state by single crystal X-ray analysis. The *in vitro* anticancer analyses showed these novel complexes suppressed the growth of breast (MCF-7), liver (HepG2) and lung (A549) cancer cells. **C2** suppressed the growth of these cells in dose-dependent manner revealed form the MTT and crystal violet cell viability assays. Moreover, **C2** was observed the most potent complex that was used further in detailed mechanistic analyses in cancer cells. **C2** showed good cytotoxic activity at 10 μM dose level as compared to cisplatin or oxaliplatin in these cancer cells. We observed morphological changes in cancer cells upon treatment with **C2**. Moreover, **C2** suppressed the invasion and migration ability of cancer cells. **C2** induced cellular senescence to retard cell growth and suppressed the formation of cancer stem cells. Importantly, **C2** showed synergistic anticancer effect with cisplatin and Vitamin C to further inhibit cell growth which suggested the potential role of **C2** in cancer therapy. Mechanistically, **C2** inhibited NOTCH1 dependent signaling pathway to suppress cancer cell invasion, migration and cancer stem cells formation. Thus, these data suggested potential role of **C2** in cancer therapy by targeting NOTCH1-dependent signaling to suppress tumorigenesis. The results obtained in this study for these novel monofunctional dimetallic Ru(η6-arene) complexes showed their high anticancer potency and this study will pave to further cytotoxicity exploration on this class of complexes.

Keywords: Ru(II)-η6-arene complexes, Tri-coordinated complexes, Ru-(*p*-cymene), Metal anticancer complexes, NOTCH1 inhibition.

1. Introduction

Cancer invasion and migration play potential roles in cancer spreading from primary to secondary organs of the body [1, 2]. Cancer stem cells formation plays a key role in drug resistance [3, 4]. Activation of cell migration and invasion along with cancer stem cells formation has been linked with tumor growth and metastasis. NOTCH1 signaling pathway plays critical role in cancer cell survival, proliferation and inhibition of apoptosis. Continuous activation of NOTCH1 signaling pathway is linked with tumor growth and drug resistance. NOTCH1 signaling promotes cancer stem cells formation and thereby favors tumorigenesis. Inhibition of NOTCH1 signaling pathway induces apoptosis, decreases cell survival, reduces the formation of cancer stem cells and decreases cell invasion and migration. NOTCH1 signaling pathway also activates several critical oncogenic signaling pathways and proteins for cancer cell growth. Inhibition of NOTICH1 signaling pathway remains thus targeting NOTCH1 signaling pathway is an attractive chemotherapeutic strategy to reduces tumor growth, invasion and migration [5-8].

Metal complexes are mandatory drug candidates and a number of metal complexes were investigated as active anticancer agents among them Pt got the first place and there are five market available drugs [9]. Similarly cancer is one of the leading causes of human mortality as because of the multiple defense mechanisms it is difficult to kill tumor cells [10-12]. Metal complexes are usually potent to kill or decrease the growth of resistant tumor cells. Cisplatin was the first line platinum-based anticancer drug approved clinically [13-16], several drawbacks were reported for cisplatin in cancer patients that diverted scientists efforts to investigate modified assemblies based platinum antitumor agents and other four drugs were approved for clinical applications [17-20]. As in all these drugs the main active function was the same platinum metal

so these issues remain more or less the same as faced by cisplatin [21-23]. Therefore, other different types of chemotherapeutic agents with potent anticancer activity were investigated, among them a variety of other metal complexes have been identified for effective cancer therapy [24-29].

The main target of platinum complexes in cancer cell is DNA that hinder its replication or cause DNA condensation by inter/intra-strand crosslinking in the parallel double strands of DNA, this DNA damage activates several apoptotic or proapoptotic processes to cause cancer cell apoptosis [30-33]. As all transition metals contain free *d*-orbitals those could coordinate with different organic donor entities including DNA, so it is hypothesized that other transition metals may also function as anticancer drug similar to platinum metal. Therefore, different other metals complexes were prepared including Ru, Cu, Ag, Co, Au, Zn, Fe and investigated for their anticancer effect in tumor cells. Among these Ru(II) got much attention due to the ability of activating different cancer cell death mechanisms [27, 34-44].

Different Ruthenium complexes were reported for their anticancer activities and photodynamic therapy (PDT) [45-49] among them Dyson and Sadler reported Ru(II)-arene complexes for the first time [50]. These complexes were found to coordinate with DNA like platinum as revealed by detailed mechanistic anticancer analyses [51-54]. KP1019, NAMI-A, RAPTA-C and RM175 (Scheme 1) showed strong anticancer activities in different types of cancer cells, also showed potential *in vivo* anticancer effect and even stronger anticancer effect was observed in cisplatin resistant cancers [49, 55, 56]. Several Ru(II) derived complexes including KP1019, NAMI-A, KP1339, RAPTA-C, RM175, TLD1433 entered clinical trials among them some are abandoned due to the low antimetastatic properties [9, 57].

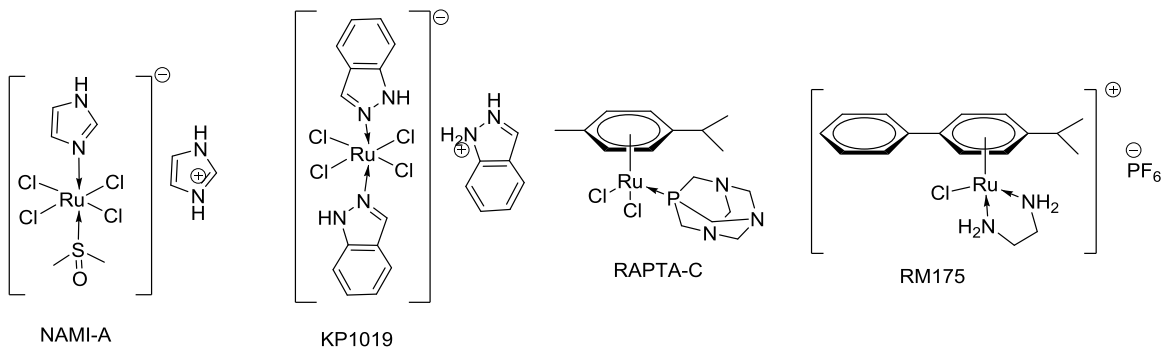

Scheme 1. Ru(II) based potential anticancer complexes

Some recent reports demonstrated that the biological activities, delivery, solubilities and side effects of Ru(II) complexes depend on the organic assembly. Therefore, large number of organic coordinating assemblies including biocompatible or other drugs-based ligands were utilized in designing of novel Ru(II) based anticancer complexes. These assemblies increased their efficacy and selectivity for different types of cancers [58-65]. A number of recent reports highlighting the biological importance of Ru(II) complexes and increasing the choices for new clinical trials based on Ru complexes [66-73]. Therefore, investigation of Ru(II) based anticancer complexes is a topic of large interest in recent time and further explorations are required on multiple aspects of Ru(II) complexes in the hope to achieve new effective and safer drugs for cancer treatments.

Mono-ligand based tri-coordinated Ru(η6-arene) complexes are seldom reported as anticancer agents, such Ru(II) complexes with bis-coordinated and mono-coordinated mixed ligands were studied for their anticancer activities, in turn these mixed ligands-based complexes were prepared in multiple steps with several stability issues [74]. Similarly, tri-coordinated Ru(η6-arene) complexes were reported for catalytic activities [75-77]. We previously reported that dimetallic Ru(II) complexes bearing salicylaldimine and η6-arene ligands depict good *in vitro* anticancer effect. Similarly, previous literature also showed the importance of metal complexes containing multiple metal atoms in anticancer biology [78]. In the current study novel bis-ONS-

tri-coordinated donor ligands were synthesized that could chelate with two Ru(II)(η6-arene). Dimetallic Ru(η6-arene) complexes (**C1**-**C4**) were isolated in excellent yields and structurally characterized by different spectroscopic and spectrophotometric methods. The structures of **C1**, **C2** and **C4** were determined in solid state using single crystal X-ray analysis. We studied their *in vitro* biological effect in multiple humans cancer cells including breast (MCF-7) non-small-cells lung carcinoma (A549) and hepatocellular carcinoma (HepG2) cells. These complexes were studied for their effect on cancer cell growth, invasion, migration, tumor spheroids formation in cancer cells. Inhibition of NOTCH1 signaling pathway and anticancer synergistic effect in presence of cisplatin or Vitamin C was investigated in cancer cells. Our results highlighted the importance of these complexes in combination therapy and points towards their importance in translational cancer research field.

2. Results and discussion

2.1 Chemistry

2.1.1. Chemical synthesis, characterization and structural aspects

Ligands **L1**-**L4** were prepared by taking 1 equivalent of dialdehyde precursor and slightly excess 2.2 equivalents of the amine precursor in refluxing ethanol. All these ligands were filtered as a solid from the cold reaction mixture bearing enough purity to be used in the next step. Ligand (**L1**-**L4**) Dichloro(*p*-cymene)ruthenium(II) dimer and NaOAc in (1 : 1.1 : 2.2) ratios were taken in CH_3OH/CH_2Cl_2 and stirred at 50 °C for 3 h (Scheme 2). After completion the mixture was evaporated using rotary evaporator. The oily solid recovered was dissolved in water and added with 4 equivalents of solid KPF_6 to precipitate a solid that was filtered and washed with water and each complex was recovered in solid form in

excellent yield. All these ligand and complexes were characterized by IR, ^{1}H, ^{13}C NMR spectroscopy, elemental analysis and high-resolution mass spectrometry (ESI Figure S1-S29). Structures of **C1**, **C2** and **C4** were analyzed in solid state by single crystal X-ray analysis. In all these di-cationic (two mono-cationic Ru atoms) complexes the ligand functioned as ONS-donor entity in which O atom of the ligand was covalently bonded to Ru while N and S donor atoms were coordinate covalently bonded to Ru bearing *p*-cymene co-ligand.

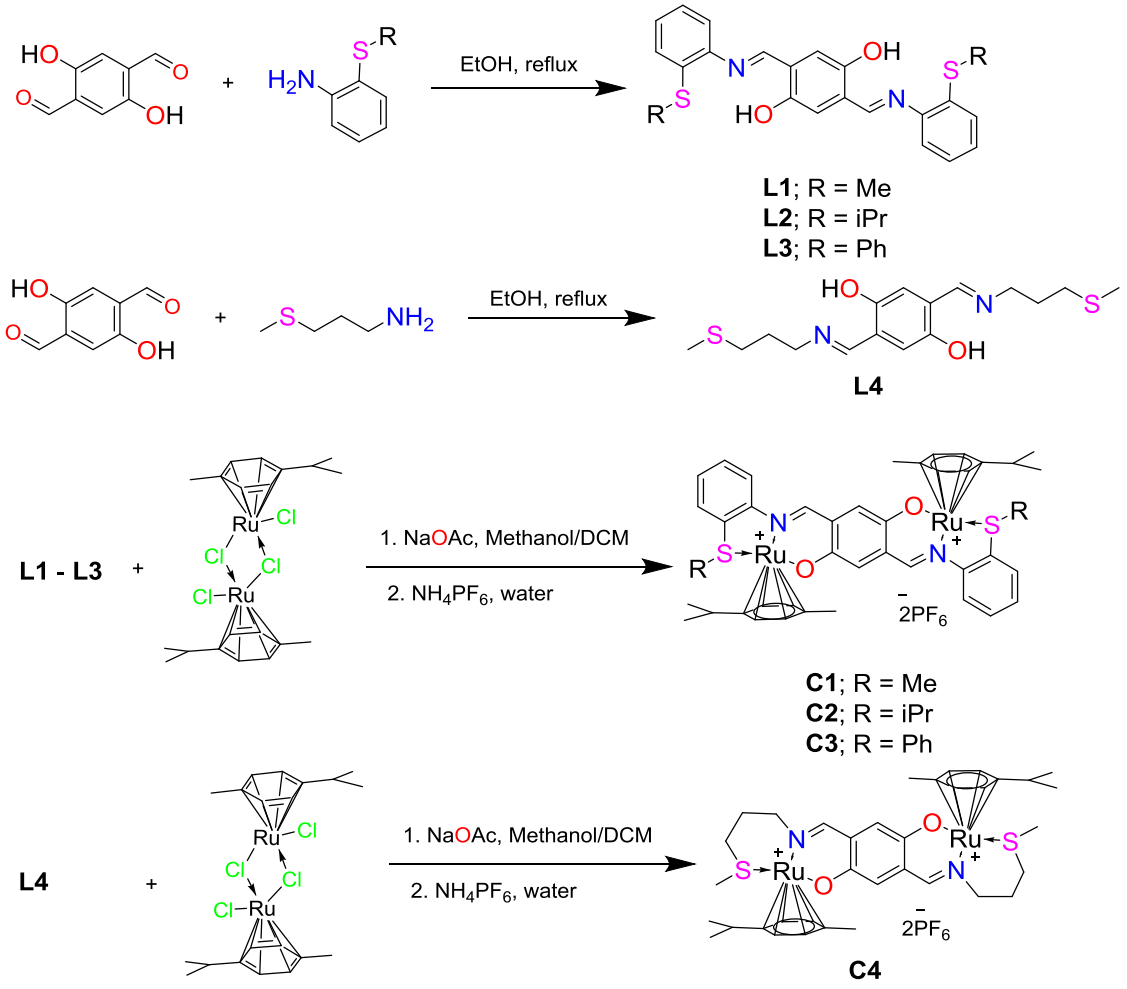

Scheme 2. Routes for the synthesis of **L1-L4** and **C1-C4**

In the ^{1}H NMR spectra of the ligand (**L1**-**L4**) the most downfield proton chemical shift was found for phenolic (OH) proton in the region 12.38-12.66 ppm (ESI Figure S1-S6). The second most downfield chemical shift was assigned to proton of the imine functions that was observed in range of 8.33-8.67 ppm. The other aromatic protons chemical shifts were found in 7.0-7.5 ppm region. For **L1** we found one singlet at 2.52 ppm that was assigned to methyls attached to S atom. In case of **L2** we found isopropyl protons signal a heptet at 3.44 and a doublet at 1.35 ppm. Similarly, for **L4** the propyl chain of the NS donor function and methyl attached to S atom were found in range of 1.98-3.74 ppm. Each ligand **L1**-**L4** was reacted with Dichloro(*p*-cymene)ruthenium(II) dimer in the presence of sodium acetate as a base to give **C1**-**C4** in excellent isolated yields. In all these complexes the chemical shifts of the respective ligand was altered due to coordination of the metal, the most prominent change observed was the disappearance of phenolic protons, that is due to the covalent bond formation between Ru and O atoms of each ligand (ESI Figure S7-S10). In case of **C1** and **C2** we observed two singlets each for one proton assigned to the imine proton of the complex while in case of **C3** and **C4** we observed one singlet for two protons of the imine function and these chemical shifts were the most downfield in each spectrum. The other aromatic protons chemical shifts of **C1**-**C3** were found in the aromatic region from 7.0-8.0 ppm while in case of **C4** a singlet for two protons of the aromatic ring was assigned at 6.71 ppm. The other potential changes were the incorporation of *p*-cymene co-ligand protons signal in the spectrum of each complex those were similar in position and in integration and assigned according to the previous literature [79]. In each complex **C1**-**C4** an asymmetric center bearing S-donor atom as stereo-center was formed and the two S atoms in one molecule got *R* and *S*

stereoisomeric structure that could also be observed in the single crystal of **C1**, **C2** and **C4**.

*2.1.2. IR analysis of **L1-L4** and **C1-C4***

FT-IR analysis for each compound **L1-L4** and **C1-C4** was performed using KBr diluted pellet, the comparative spectra were plotted in Figure 1 below and separate spectra for each compound with peaks positions were given in the (ESI Figure S20-S29). Each peak in the IR spectrum was assigned in comparison with previous literature for related compounds. The most prominent peak in each **L1-L4** and **C1-C4** around 1600 cm^{-1} region was assigned to stretching of imine C=N bond. Compared to the corresponding ligand, each complex (**C1-C4**) showed a big and broad peak around 850 cm^{-1} that was the stretching frequency of PF_6 anions that confirmed ions exchange form chloride to PF_6.

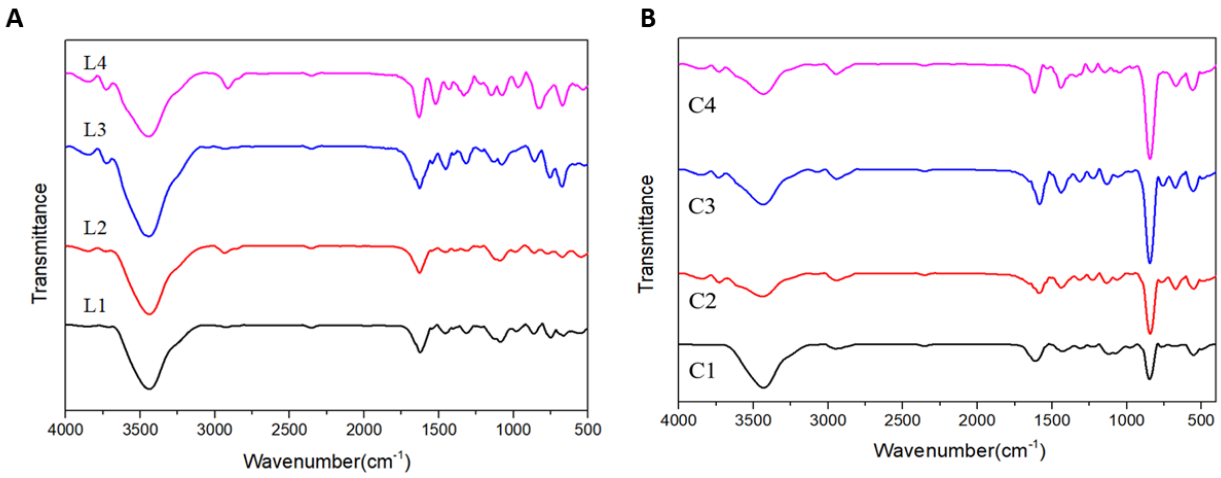

Figure 1. Comparative FT-IR Spectra plot of **L1-L4** (A) and **C1-C4** (B)

*2.1.3. Single crystal study of **C1**, **C2** and **C4***

X-ray quality crystals of **C1**, **C2** and **C4** were obtained by slow diffusion of diethyl ether to a solution of each complex in acetonitrile, several attempts to grow single crystal for **C3** failed we obtained crystalline powder bearing no suitable single crystal for X-ray

analysis. The ORTEP plot of each complex (**C1**, **C2** and **C4**) was displayed in Figure 2 and the solid-state structure features were summarized in Table 1. **C1** crystallized in monoclinic while **C2** and **C4** showed triclinic crystal system bearing P21/c, P-1 and P-1 space group respectively. The main salicylaldimine ligand coordinated to Ru(II) through ONS-donor atoms while the other coordinates of the metal were completed by *p*-cymene co-ligand. Each complex was a di-cationic specie in which each Ru(II) was single positively charged with one PF_6 counter anion.

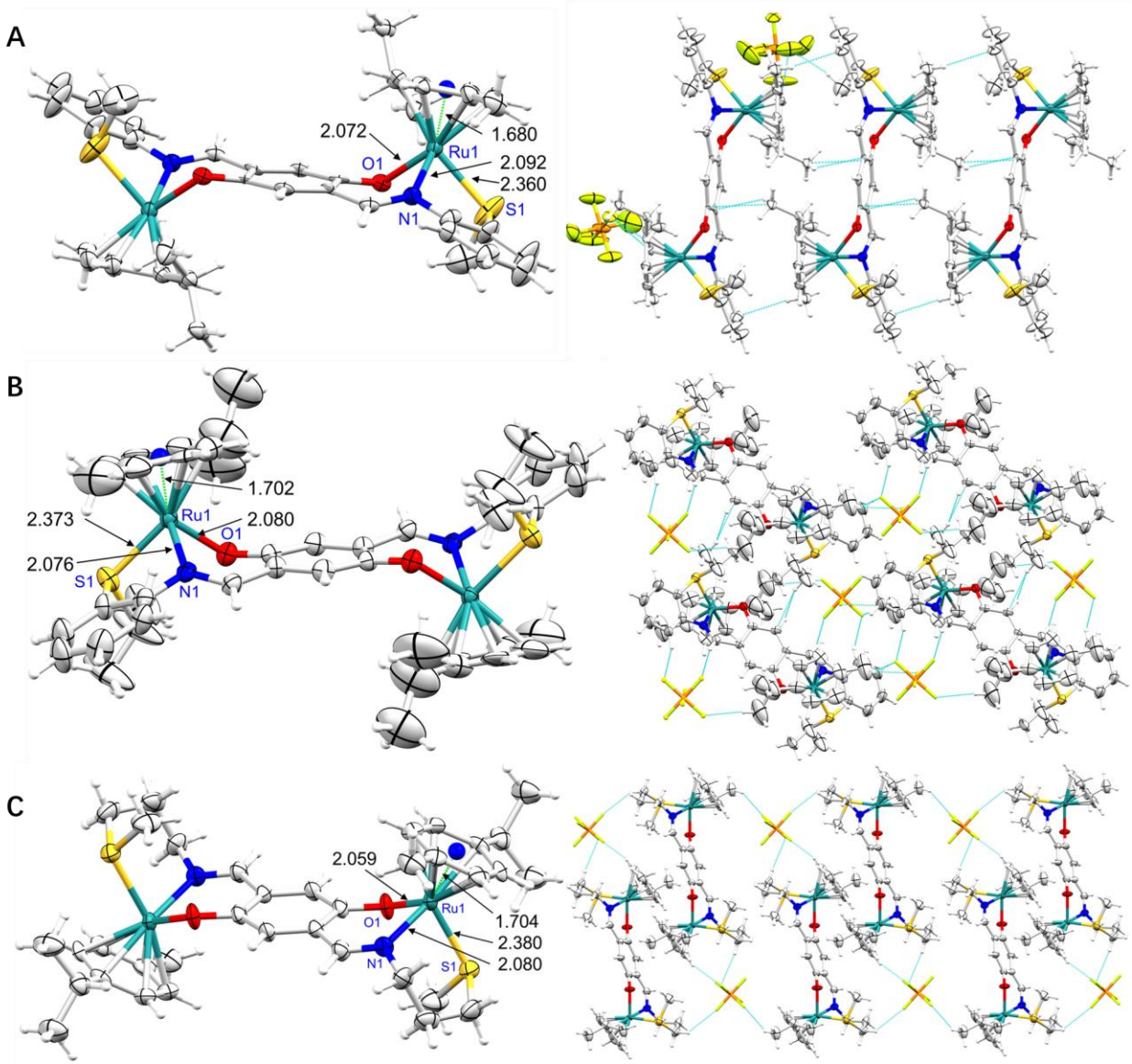

Figure 2. ORTEP plot of **C1**(A), **C2**(B) and **C4**(C) at 50% probability displacement of the thermal ellipsoids; Single molecule showing labelled atoms coordinated to Ru and the bond length between each of the coordinated atom to Ru (left), short bonding among molecules that facilitated 3D arrangement in crystal packing (right).

Table 1. Structure refinement parameters of **C1**, **C2**, and **C4**

	C1	**C2**	**C4**
Empirical formula	$C_{42}H_{46}F_{12}N_2O_2P_2Ru_2S_2$	$C_{46}H_{54}F_{12}N_2O_2P_2Ru_2S_2$	$C_{36}H_{50}F_{12}N_2O_2P_2Ru_2S_2$
Formula weight	1167.01	1223.11	1098.98
Temperature (K)	149.99(10)	219.99(10)	292.98(10)
Crystal system	monoclinic	triclinic	triclinic
Space group	$P2_1/c$	P-1	P-1
Unit cell dimensions			
a (Å)	7.8403(8)	9.2180(6)	8.4308(7)
b (Å)	14.221(2)	9.8968(9)	11.2598(9)
c (Å)	20.498(2)	13.8259(14)	11.5491(10)
α (°)	90	91.794(8)	96.474(7)
β (°)	86.310(9)	90.308(7)	102.202(7)
γ (°)	90	98.244(6)	97.550(6)
Volume ($Å^3$)	2280.8(5)	1247.61(19)	1051.06(16)
Z	2	1	1
Density (calculated) (mg/m^3)	1.699	1.628	1.736
Absorption coefficient (mm^{-1})	0.912	0.838	0.983
F(000)	1172.0	618.0	554.0
Crystal size (mm^3)	0.13 × 0.12 × 0.11	0.13 × 0.11 × 0.08	0.12 × 0.11 × 0.09
Theta range for data collection (°)	3.982 to 49.972	4.16 to 50.132	4.796 to 49.996
Index ranges	$-7 \le h \le 9$, $-16 \le k \le 16$, $-23 \le l \le 24$	$-10 \le h \le 10$, $-11 \le k \le 11$, $0 \le l \le 16$	$-8 \le h \le 10$, $-13 \le k \le 13$, $-10 \le l \le 13$
Reflections collected	11633	4392	6842
Independent reflections	4015 [R_{int} = 0.0682, R_{sigma} = 0.0887]	4392 [R_{int} = 0.0522, R_{sigma} = 0.1092]	3684 [R_{int} = 0.0642, R_{sigma} = 0.0818]
Data / restraints / parameters	4015/254/293	4392/71/313	3684/0/266
Goodness-of-fit on F^2	1.253	1.173	1.047
Final R indices [I>2sigma(I)]	R_1 = 0.1327, wR_2 = 0.2454	R_1 = 0.1186, wR_2 = 0.2936	R1 = 0.0599, wR2 = 0.1579
R indices (all data)	R_1 = 0.1527, wR_2 = 0.2543	R_1 = 0.1275, wR_2 = 0.2991	R1 = 0.0748, wR2 = 0.1730

Largest diff. peak and hole (e.Å^{-3})	2.03/-1.50	2.67/-2.88	1.35/-0.94

[a] $R_1 = \Sigma_{\text{all reflections}} |F_0 - F_c| / \Sigma_{\text{all reflections}} |F_0|$, [b] $wR_2 = [\Sigma w(F_0^2 - F_c^2)^2 / \Sigma (w(F_0^2)^2)]^{1/2}$.

In these complexes each Ru metal depicted a three-legged piano-stool conformation bearing *p*-cymene and tricoordinated main salicylaldimine ligand that is coordinated to Ru(II) through ONS donor atoms. Table 2 and Figure 2 summarized selected bond lengths and angles of each atom coordinated to Ru and centroid of the *p*-cymene in **C1**, **C2** and **C4**. The respective bond distances for each metal and coordinated atoms in each complex (**C1**, **C2** and **C4**) including Ru(1)-O(1), Ru(1)-N(1), Ru(1)-S(1) were found nearly similar in these complexes and found in the range of 2.06-2.08 for Ru(1)-O(1), 2.076-2.092 for Ru(1)-N(1) and 2.361-2.3798 for Ru(1)-S(1) (Figure 2 and Table 2 entry 1-3). The bond distance between the centroid of *p*-cymene and Ru(1) in **C1** was 1.68 Å while for **C2** and **C4** it was 1.702 and 1.704 respectively (Figure 2 and Table 2 entry 4). The bond angles between ONS coordinated atoms of the main ligand and Ru(II) were given in Table 2, the smallest angle observed was ∠N(1)-Ru(1)-S(1) in **C1** and **C2** while ∠O(1)-Ru(1)-N(1) was found the smallest one in **C4** that could be due to the flexibility of the alkane chain in the amine part of the ligand that arranged itself to the most stable position (Table 2 entry 5-7). While ∠O(1)-Ru(1)-S(1) was observed the biggest angle on each Ru atom in each of these complexes. (Table 2 entry 5).

Table 2. Selected bond lengths (Å) and angles (°) around Ru atom in each complex

Entry	**Bond/Angle**	**C1**	**C2**	**C4**
Bond length (Å) for each metal in each complex				
1	Ru(1)-O(1)	2.073(5)	2.080(10)	2.060(4)
2	Ru(1)-N(1)	2.092(6)	2.076(11)	2.080(5)
3	Ru(1)-S(1)	2.361(3)	2.373(4)	2.3798(17)
4	Ru(1)-Centroid of *p*-	1.680	1.702	1.704

	cymene			
Bond angle (°) for each metal in each complex				
5	∠O(1)-Ru(1)-S(1)	93.64(16)	93.5(3)	87.78(15)
6	∠O(1)-Ru(1)-N(1)	80.8(2)	80.6(4)	85.64(19)
7	∠N(1)-Ru(1)-S(1)	79.33(19)	80.0(3)	86.15(15)

In crystal packing of **C1** 1D chain formation of molecules was observed through close contact of the propyl group of *p*-cymene co-ligand of one molecule with the phenylene ring of the other nearby molecule (Figure 2), further interaction of PF_6 anions with different hydrogen atoms helped in arrangement of the molecules in 3D crystal packing. While in **C2** propyl group attached to S donor atom formed close contacts with central phenylene and helped molecules arranged in head to tail manner, further bonding with PF_6 anions arranged molecule in 3D crystal packing (Figure 2). In case of **C4** close interaction between propyl group of *p*-cymene with the same group of the neighboring molecule arranged molecules in head to tail manner and PF_6 anions interaction with different hydrogen of the complex stabilized molecules to arrange in 3D crystal packing (Figure 2).

2.1.4. Stability analysis

The stability of a bioactive metal complex in solution state is important feature that determines hydrolysis or replacement of one or more donor ligand with the organic solvent or water molecule in which it is dissolved and in turn affect its anticancer activity [49]. Previously related Ru(II)-arene or other metal anticancer complexes were analyzed for their stabilities in solution state by different techniques including UV, ^{1}H NMR spectroscopy and/or mass spectrometry. Similarly, the aquation, interaction with target biomolecule and cytotoxicity in solution state behavior was also studied [80-82]. In our previous studies we used ^{1}H NMR spectroscopy and

HR-MS to determine solution state stabilities of Ru or Pt anticancer complexes [79, 83-86]. In the current study we determined the stabilities of reference complexes **C2** and **C4** by ^{1}H NMR spectroscopy. **C2** was analyzed in different ratio of solvents viz pure DMSO-d_6, DMSO-d_6/D_2O (4:1) and DMSO-d_6/D_2O (3:2) solvent mixtures (Figure 3A-D). We found in pure DMSO-d_6 *p*-cymene ligand was slowly replaced by DMSO-d_6 and after 14 days the replacement process was completed (Figure 3A-B). We clearly see the changes in the protons chemical shifts and peaks for free *p*-cymene were observed. We performed HR-MS analyses in acetonitrile and also in DMSO as a solvent, the mass spectrum in acetonitrile showed a peak for *m/z* 467.0858 assigned to M - 2PF_6 (ESI Figure S16) while in DMSO we observed a singly charged specie at *m/z* 1044.9425 assigned to M - 2*p*-cymene + 3DMSO – PF_6 (ESI Figure S19) showing the replacement of *p*-cymene with 3 DMSO molecules (Scheme 3). The increasing ratio of water in the solvent mixture decreased the dissociation of *p*-cymene co-ligand from this complex this could be a kind of protection of the complex from being attacked by the DMSO ligand and may be presented as the surrounding of a cationic Ru(II) complex by water deprived DMSO to reach the metal center to substitute *p*-cymene (Figure 3C-D). We prepared solution of each complex in DMSO/D_2O (3:2) and used them in biological analyses.

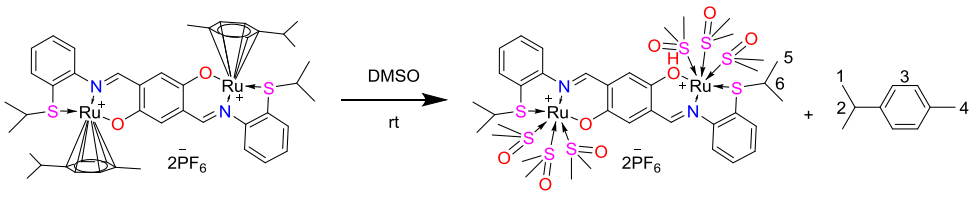

Scheme 3. Replacement of *p*-cymene co-ligand of **C2** by DMSO

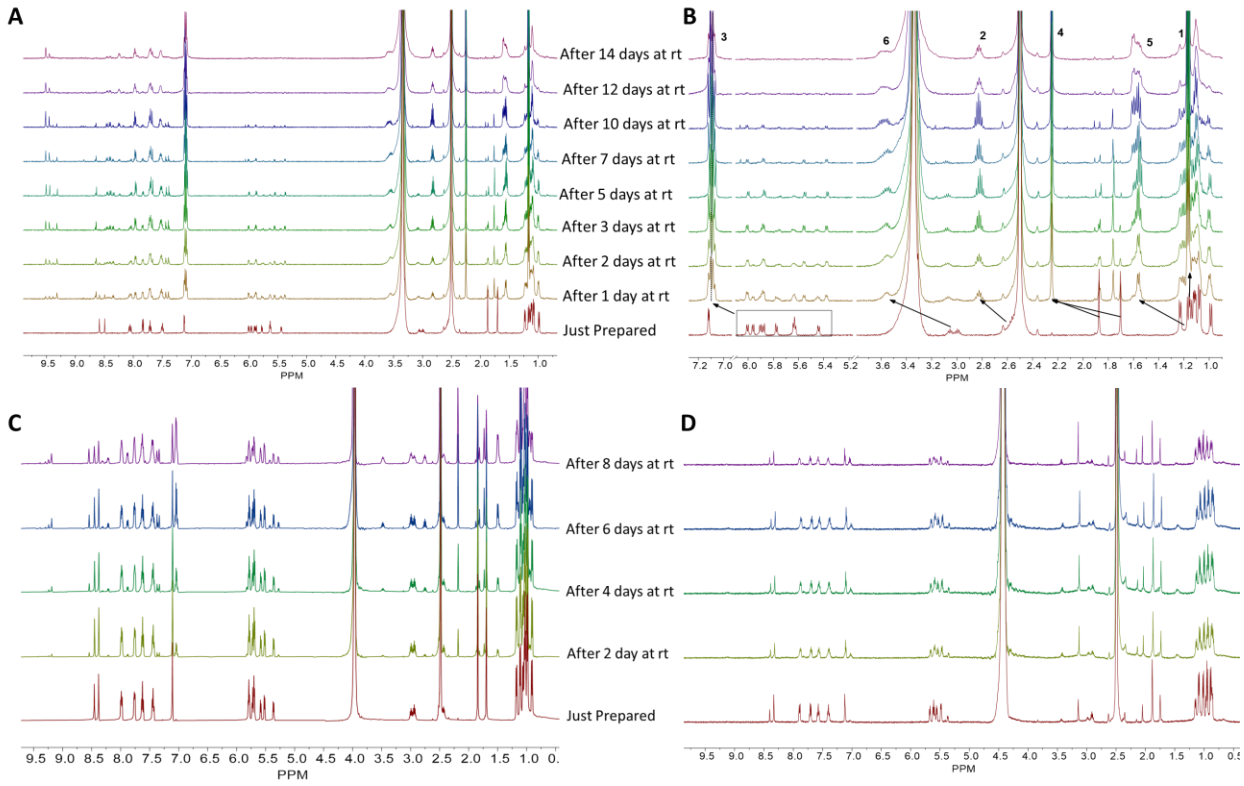

Figure 3. Stability analyses of **C2**; (A) Comparative spectra plot in pure DMSO-d_6 (B) Partial ^{1}H NMR plot of spectra in (A) arrow showed shifting of protons chemical shifts due to new species formation while the number represented the protons chemical shifts mentioned in scheme 3, (C) Comparative spectra plot in DMSO-d_6/D_2O (4:1) mixture (D) Comparative spectra plot in DMSO-d_6/D_2O (3:2); In each experiment 2 mg of **C2** was dissolved in the respective solvent and analyzed by ^{1}H NMR spectroscopy over the mentioned time points.

Repeated analyses of **C4** in DMSO/D_2O (2:3) mixture over 7 days showed no distinguishable changes in all the protons chemical shifts of **C4** (Figure 4). Similarly, we did not observe the characteristic protons chemical shifts of free *p*-cymene co-ligand. These analyses showed the uniformity **C4** under these conditions over a week. We observed the substitution of labile ligand (*p*-cymene) in case of **C2**, in our previous study we found hydrolysis of the ancillary chloride ligand [79] but in case of **C4** we did not observe any dissociation or replacement of the ligand by solvent molecules (DMSO) which is a strong donor solvent that easily coordinate with the metal [84, 87]. Compared to **C2** greater stability of **C4** may be due to the alkane chain connecting NS

donor atoms that could orientate in the most stable form due to flexibility of the chain as compared to the rigid flatter aromatic ring of benzene in **C2**. We used the same solvent to prepare stock solutions for biological studies.

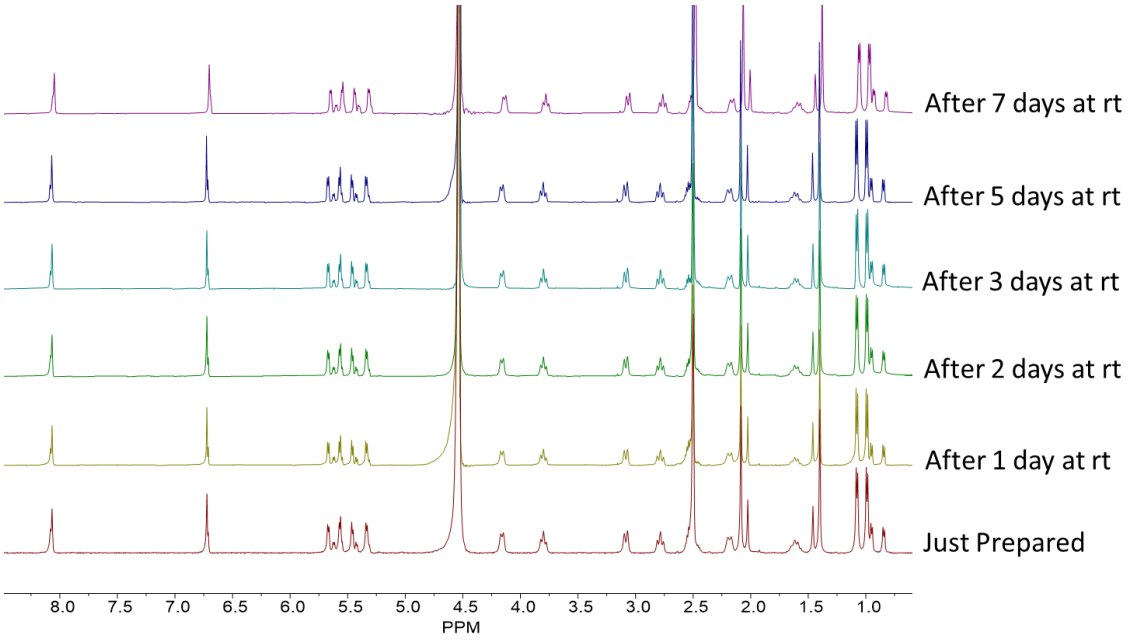

Figure 4. Stability analyses of **C4**; 2 mg of **C4** was dissolved in DMSO-d_6/D_2O (3:2) mixture and analyzed by ^1H NMR spectroscopy over the mentioned time points.

2.2. Anticancer activities

2.2.1. Inhibition of cancer cell growth

The *in vitro* antiproliferative effect of **C1**–**C4** was analyzed on human breast cancer (MCF-7), human lung cancer (A549) and human liver cancer (HepG2) cell lines. These cancer cells were exposed to 20 μM dose of each **C1**–**C4** or DMSO as negative control for 48 h and analyzed by MTT assay (Figure 5A-C). Result showed all these complexes showed potential anticancer effect in all kind of these cancer cells. Among them **C2** was the most active complex in all these cancer cells and the effect of **C2** was comparable to **C4**, **C3** showed lower effect compared to **C2** and **C4**, while **C1** displayed moderate effect on the growth of these cancer cells. All these results

demonstrated these complexes to be active anticancer agent as they decreased the growth of cancer cells.

C2 was the most effective complex, we selected **C2** as reference complex to proceed detailed mechanistic studies in cancer cells. The dose-dependent growth suppression of cancer cell by **C2** was determined adding different concentrations of **C2** to all these three types of cancer cells over 24 or 48 h of exposure time (Figure 5D-F). The result showed dose-dependent inhibition of cancer cell growth determined by MTT assay that is further increased with increasing exposure time. Similarly, crystal violet assays results also affirmed the dose-dependent inhibition of cancer cell growth in all these three types of cancer cells (Figure 5G-J).

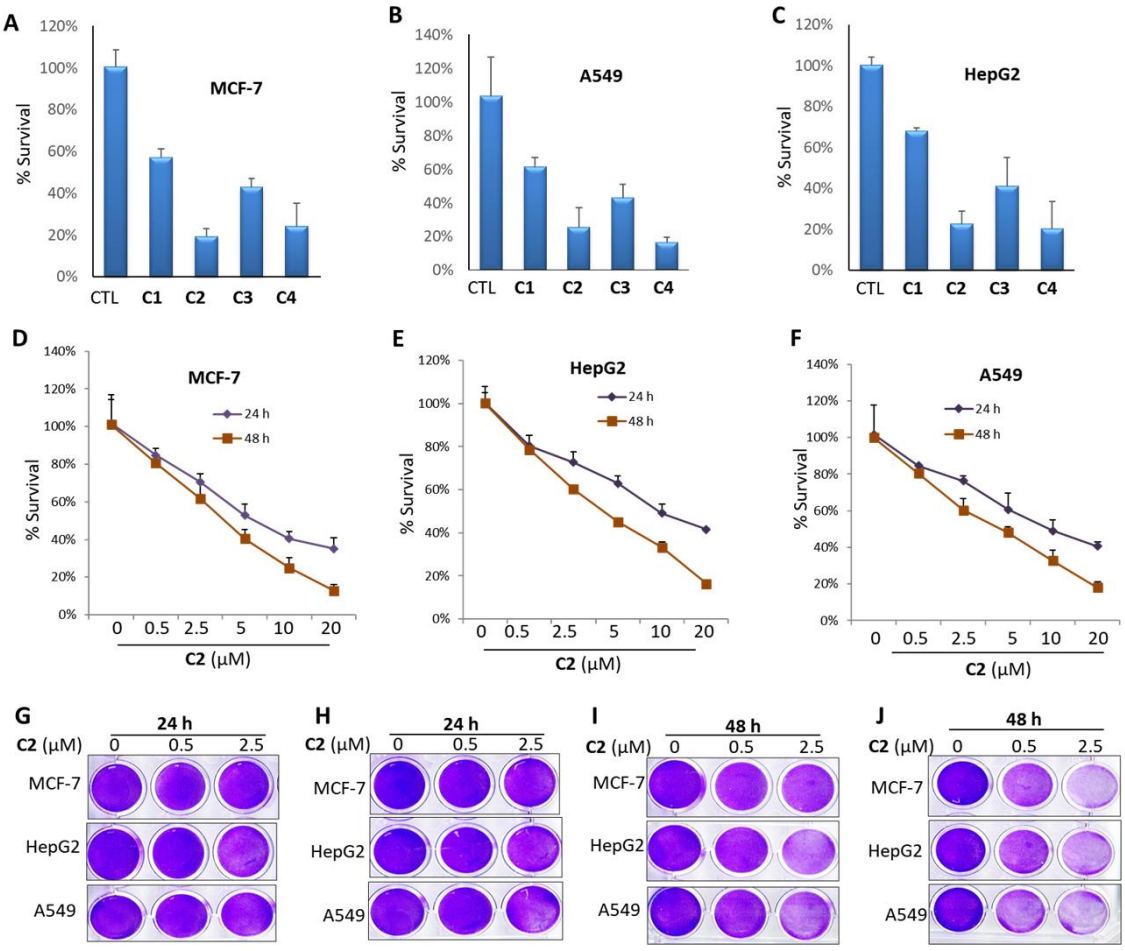

Figure 5. Ru(II) complexes inhibit cancer cell growth; (A-C) MCF-7, HepG2 and A549 cells were treated with DMSO and 20 µM of each **C1**-**C4** for 48 h and cell viability was determined by MTT assay. Dose dependent inhibition of cell growth by **C2**; (D-F) MCF-7, HepG2 and A549 cells were treated with DMSO and indicated concentrations of **C2** for 24 and 48 h and cell viability was determined by MTT assay, (G-J) MCF-7, HepG2 and A549 cells were treated with DMSO or indicated concentrations of **C2** for 24 and 48 h and cell viability was determined by crystal violet assay.

*2.2.2. Comparative cell growth inhibition by **C2** with cisplatin and oxaliplatin*

Cisplatin is the first line market available platinum-based anticancer drug while oxaliplatin is the recently approved anticancer drug used in treatment of multiple cancers. The anticancer effect of reference complex **C2** was compared with these drugs in MCF-7, A549 and HepG2 cancer cells (Figure 6A-F). The results showed higher cell growth inhibition by **C2** as compared to positive controls cisplatin or oxaliplatin in all these cancer cells. These results showed **C2** was more effective at 10 µM concentration as compared to cisplatin or oxaliplatin in all these cancer cells. Moreover we also performed this comparative study by crystal violet assays and the results were similar to MTT assay. Thus, both MTT and crystal violet data suggesting that **C2** is more effective as compared to cisplatin and oxaliplatin. The effective killing of cancer cells as compared to both market available drugs highlighting the importance of these Ru(II) dimetallic complexes to be investigated as alternative anticancer agents in drug discovery.

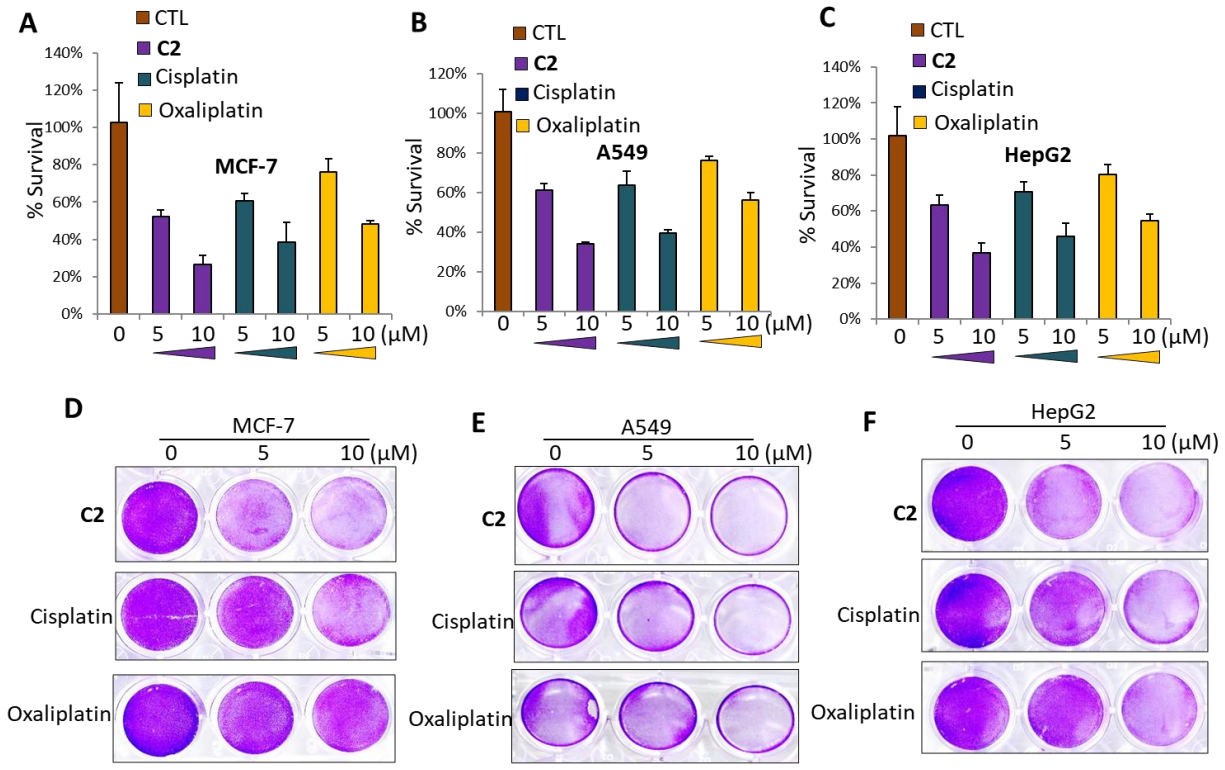

Figure 6. Comparison of cytotoxicity of **C2** with cisplatin and oxaliplatin; A-C, MCF-7, HepG2 and A549 cells were treated with DMSO, **C2**, cisplatin or oxaliplatin for 48 h and cell viability was determined by MTT assay, (D-F) MCF-7, HepG2 and A549 cells were treated with mentioned concentration of DMSO, **C2**, cisplatin or oxaliplatin for 48 h and cell viability was determined by crystal violet assay.

2.2.3. Effect on cancer cells morphology

Cell morphology is an important feature of cancer cells that shows cancer cell growth and apoptosis. Cancer cells become round after drug treatment generally undergo apoptosis. The effect of **C2** on cell morphology was investigated using different human cancer cells in dose-dependent manner. A549, MCF-7 and HePG2 human cancer cells were treated with different doses of **C2** and cisplatin as positive control and cells images were taken under bright field (Figure 7A-C). Detectable morphological changes were observed in all these cancer cells treated with **C2** in comparison to cisplatin. These results suggested that treatment of these cancer cells with **C2** induced cell death as the cancer cells appears to be apoptotic after treatment with different doses of **C2**. These results highlighted the importance of **C2** in multiple human cancer

cells death initiation via apoptosis. Importantly, these results also suggested that **C2** is more cytotoxic than cisplatin in multiple human cancers as evidenced by the changes in cancer cell morphology.

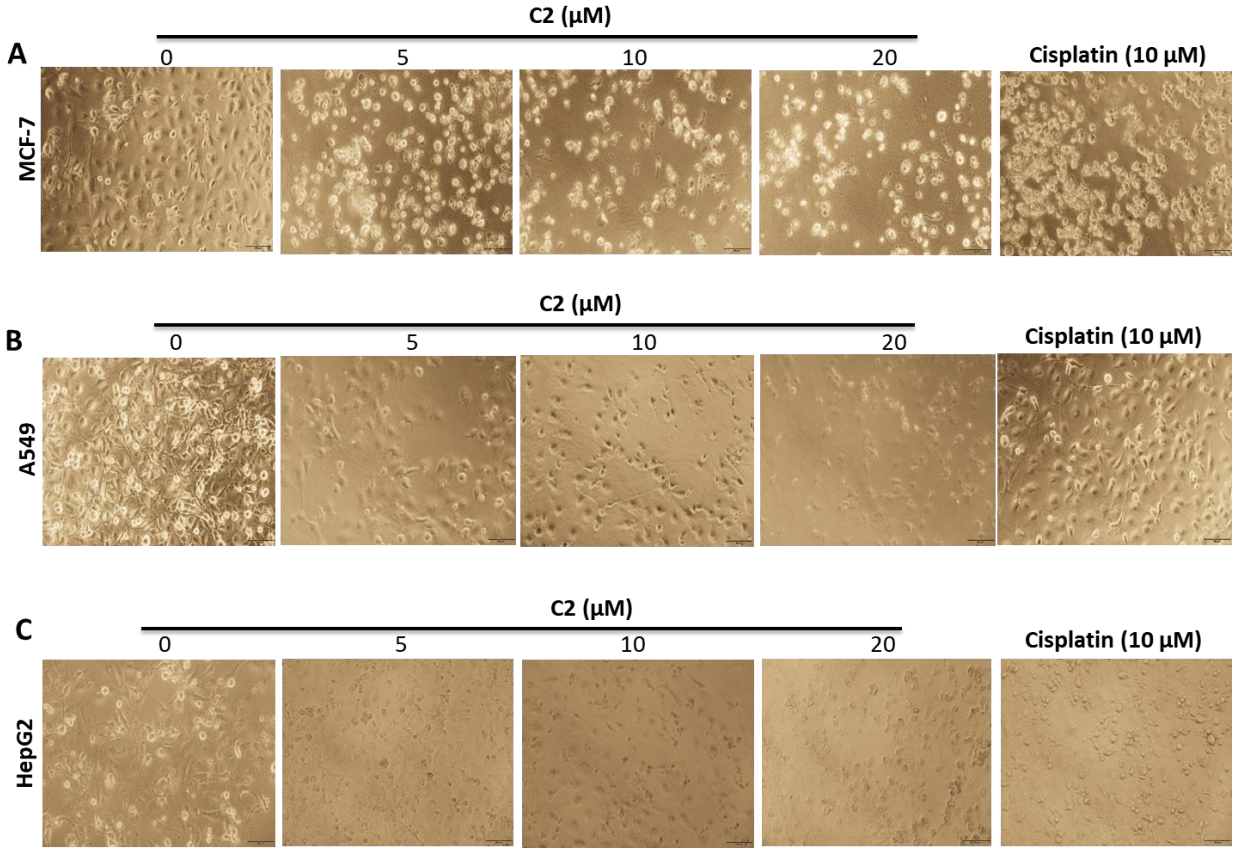

Figure 7. C2 causes cell death in cancer cells; (A-C) MCF-7, HepG2 and A549 cells were treated with DMSO and different concentration of **C2** for 48 h and cell morphology was detected under bright field imaging.

*2.2.4. **C2** induces cellular senescence in cancer cells*

Cellular senescence plays important role in cancer cells retardation and reduces tumor cell growth, invasion and metastasis. Anticancer agents promote cellular senescence are considered important in the field of cancer therapy. We investigated the effect of **C2** on cellular senescence in multiple human cancer cells including HepG2, MCF7 and A549 cells (Figure 8A-D). Thus,

we treated cancer cells with **C2** for 3 days and observed a strong induction in cellular senescence as compared to DMSO treated cells (negative control). Our data suggested that **C2** promoted cellular senescence and thereby induced cancer cells growth arrest to decrease cell proliferation, invasion and migration. These results highlighted the importance of **C2** in induction of cellular senescence in different human cancer cells.

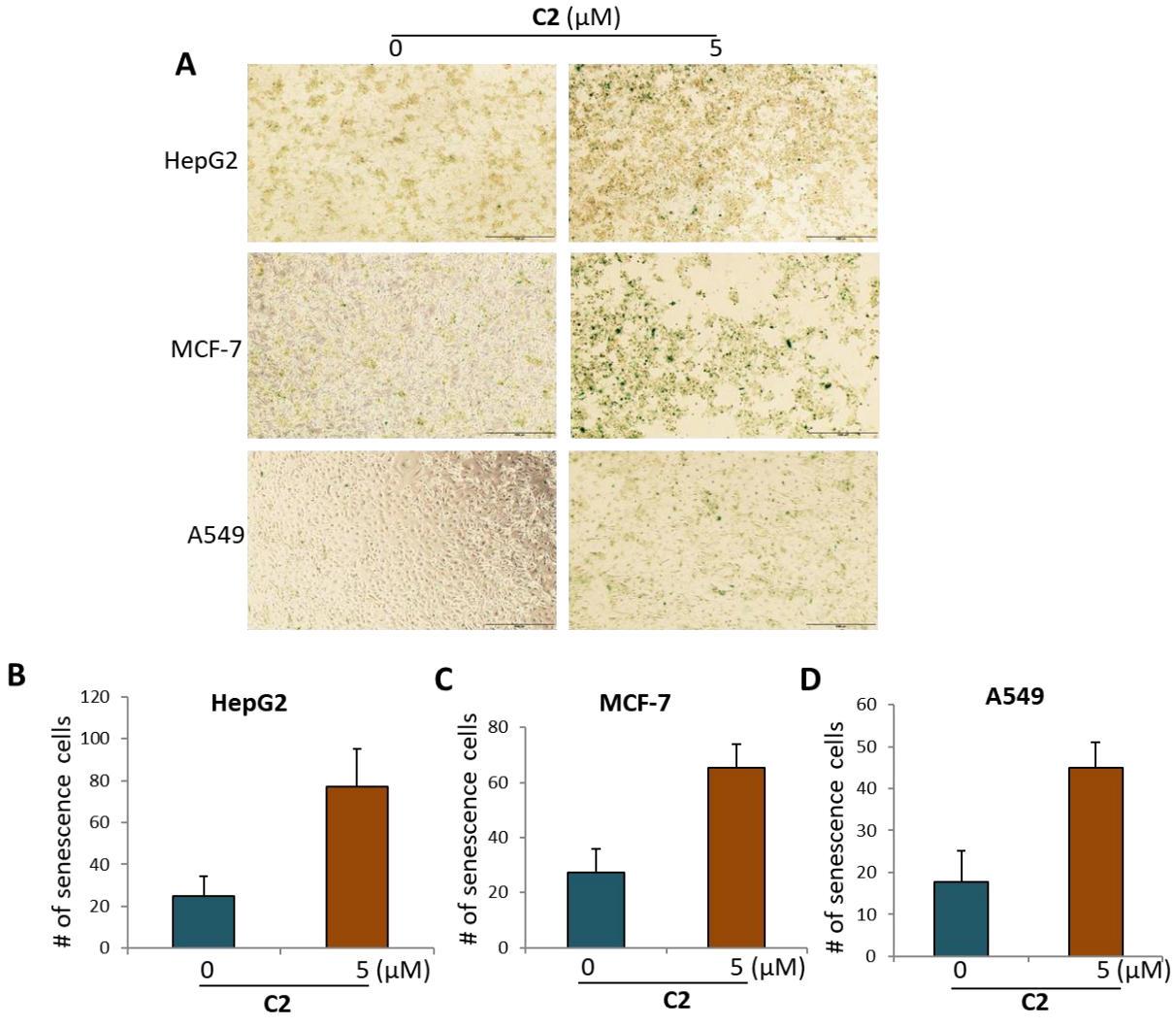

Figure 8. C2 induces cellular senescence in cancer cells; (A) MCF-7, HepG2 and A549 cells were treated with DMSO and 5 μM of **C2** for 72 h and cellular senescence was observed under microscope. (B-D) Graphical representation of data from figure for MCF-7, HepG2 and A549 cancer cells.

2.2.5. Suppression of cancer stem cells formation

Tumor spheroids formation is important in drug resistance and cancer cells stemness. Cancer stem cells formation also promotes drug resistance and tumor burden. Therefore, we investigated the effect of **C2** on cancer stem cells/tumor spheroids formation in different human cancer cells including MCF-7, A549 and HepG2 cells (Figure 9A-D). Our data showed that **C2** suppressed cancer stem cells/tumor spheroids formation of MCF-7, A549 and HepG2 cancer cells that suggested an important role of **C2** in cancer stemness inhibition. These results suggested important role of **C2** in inhibition of tumor spheroids and reduction of cancer stem cells formation. These results also points towards the role of **C2** in inhibition of formation of circulating tumor cells.

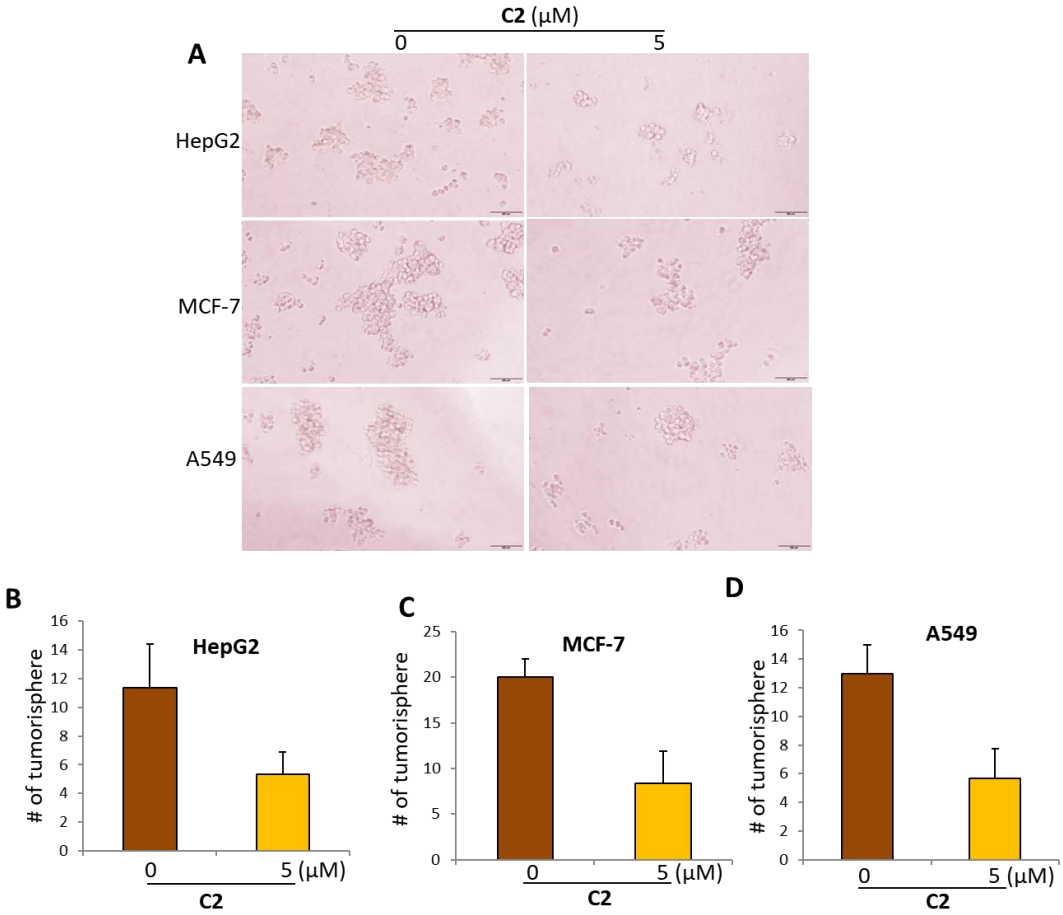

Figure 9. C2 suppresses cancer stem cells formation; (A) MCF-7, HepG2 and A549 cells were treated with DMSO negative control and 5 µM of **C2** for 5 days and cancer stem cells formation was observed under microscope. (B-D) Graphical representation of data from figure for MCF-7, HepG2 and A549 cancer cells.

2.2.6. Inhibition of cancer cells migration

Cancer cell migration plays important and key role in metastasis and its inhibition has been linked with decreased metastatic potential of cancer cells. Therefore, we investigated the effect of **C2** on cell migration in different human cancer cells including MCF-7, A549 and HepG2 cells (Figure 10A-C). Interestingly, we observed MCF-7, HepG2 and A549 cancer cells treated with **C2** showed decreased cell migration in comparison to the control cells treated with DMSO. These results suggest that **C2** has potential to suppress cell migration ability of different human cancers. These results also showed the importance of **C2** in suppression of cancer cell growth and thereby reduces tumor metastasis.

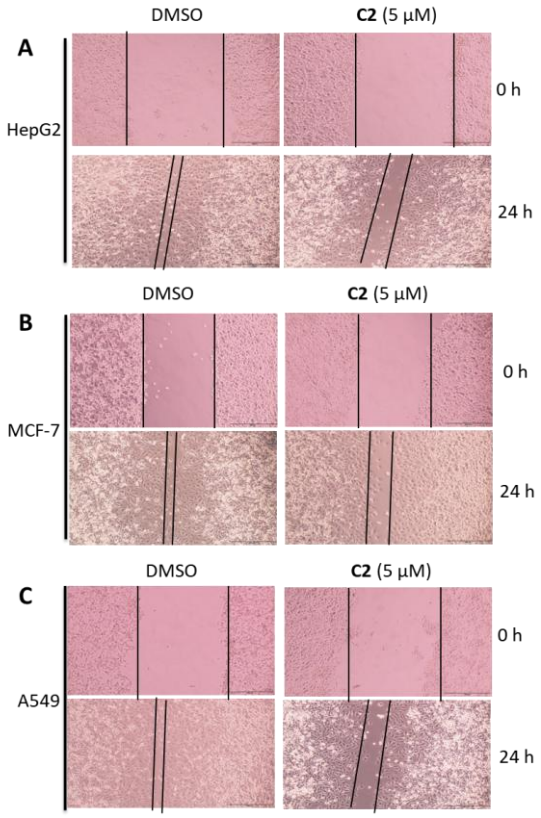

Figure 10. C2 suppresses wound healing in cancer cells; (A-C) MCF-7, HepG2 and A549 cells were treated with DMSO or 5 µM of **C2** for 24 h, then scratched and cell migration was observed after 24 h.

2.2.7. Inhibition of cancer cell invasion

Cancer cell invasion play pivotal role in metastasis and its inhibition point toward the suppression of cancer progression. Based on its important role in cancer spreading, we checked the effect of **C2** on cell invasion in MCF-7, A549 and HepG2 cells (Figure 11A-C). Data suggested that MCF-7, A549 and HepG2 cancer cells treated with **C2** showed decrease cell invasion ability as compared to the control cells. These results suggested potentials of **C2** to suppress cancer cell invasion which in turn reduces metastatic potential of cancer cells. Blocking invasion of cancer cells by **C2** also suggested its importance in tumor metastasis.

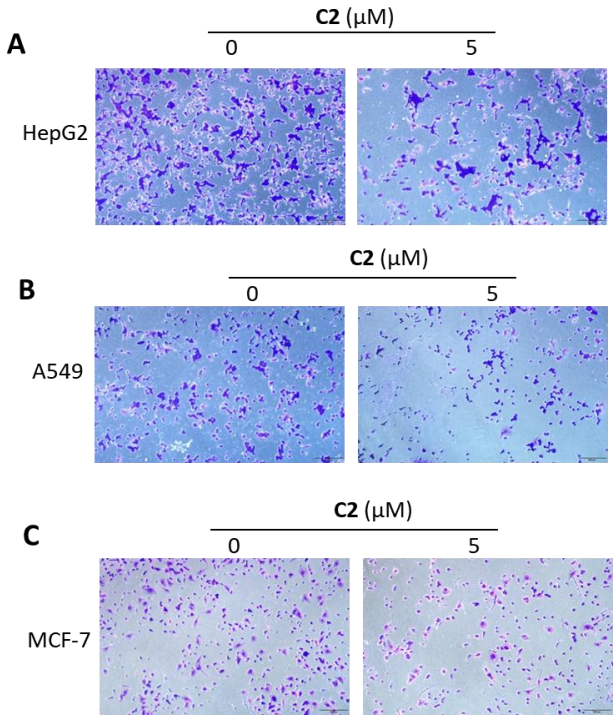

Figure 11. C2 suppresses invasion ability of cancer cells; (A-C) MCF-7, HepG2 and A549 cells were treated with DMSO and 5 µM of **C2** for 24 h and then subjected to invasion assay.

*2.2.8. **C2** synergize anticancer effect with vitamin C*

Vitamin C has been shown to play important roles in cancer inhibition by inducing cell death [88, 89]. Vitamin C also play a role to suppress invasion and metastasis [90, 91]. Therefore, we decided to check the combined effect of vitamin C and **C2** on MCF-7, A549 and HepG2 cancer cell growth (Figure 12A-D). We observed inhibition of cell growth in these cancer cells when they were treated with Vitamin C or **C2** alone. Interestingly, combined treatment of Vitamin C and **C2** showed stronger effect on cell proliferation in comparison to single compound treatment. These results suggested that **C2** synergize the anticancer effect with vitamin C to further induce cell death in MCF-7, A549 and HepG2 cells. This data also highlighted the potential and novel role of **C2** in combination with vitamin C to promote cancer cell death. These results points towards the importance of **C2** in combination with natural compounds such as Vitamin C in the field of cancer therapy.

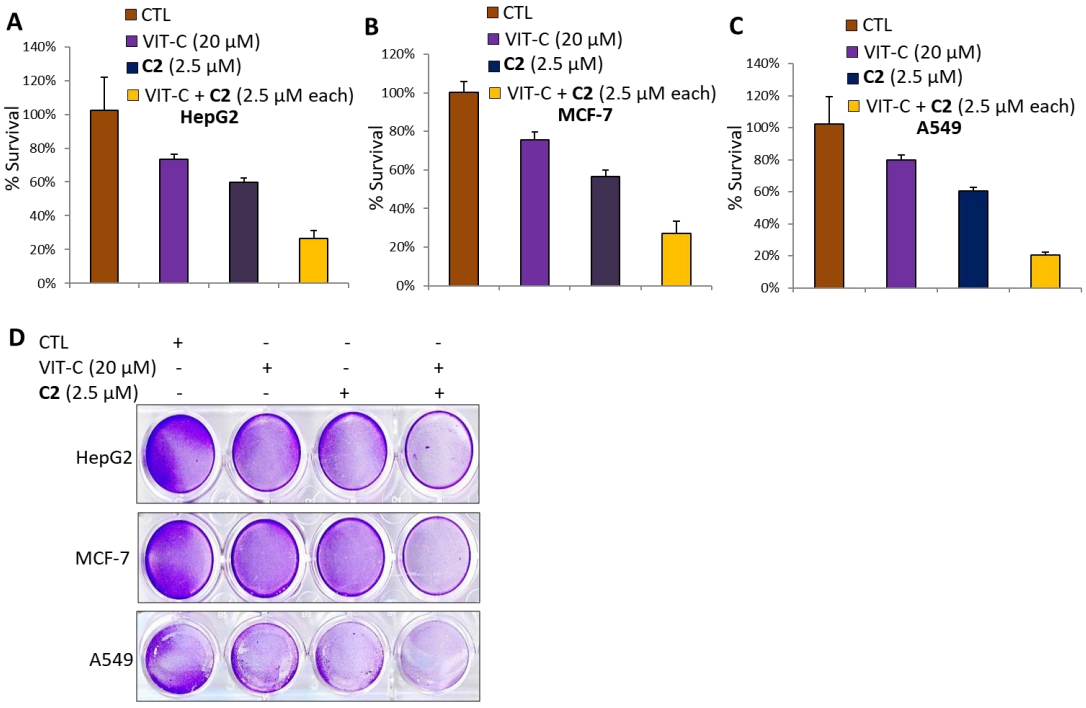

Figure 12. Combination study of **C2** with Vitamin C in cancer cells; (A-C) MCF-7, HepG2 and A549 cells were treated with DMSO, 2.5 µM of **C2**, 20 µM of vitamin C independently or in combination for 48 h and cell viability was determined by MTT assay. (D) MCF-7, HepG2 and A549 cells were treated with DMSO, 2.5 µM of **C2**, 20 µM of vitamin C independently or in combination for 48 h and cell viability was determined by crystal violet assay.

*2.2.9. **C2** synergize effect with cisplatin*

Cisplatin is an important first generation effective chemotherapeutic agent, several studies showed combined treatment of cisplatin with other anticancer agents [92-94]. Therefore, we investigated the effect of cisplatin and **C2** combined on MCF-7 cell, MTT assay showed that **C2** and cisplatin alone treatments inhibited MCF-7 cells growth (Figure 13A-B). However, combined treatment effect of **C2** and cisplatin was much stronger than the single treatment with each cisplatin or **C2**. These results suggested potential mechanism by combined treatment of cisplatin and **C2** to trigger cell death of MCF-7 cells. This data also suggested that **C2** has potentials to synergize anticancer effect with other anticancer agents such as cisplatin, which further increase the importance of **C2** in the field of cancer therapy.

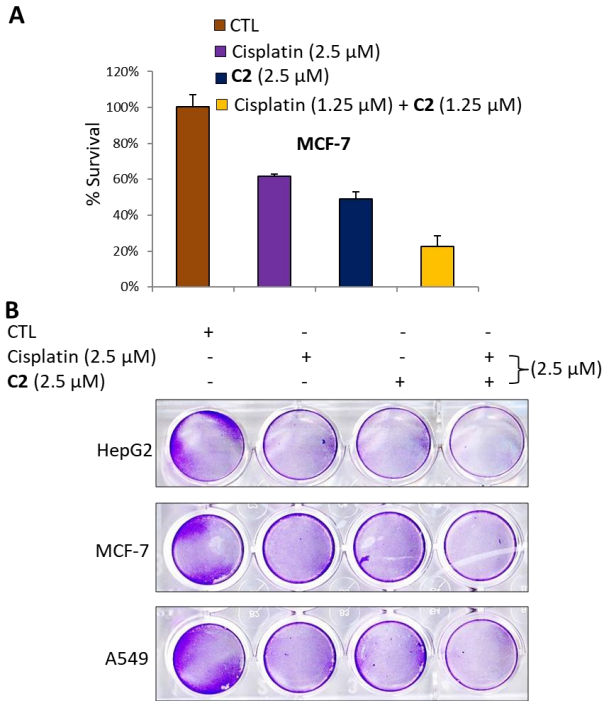

Figure 13. Combination study of **C2** with cisplatin in MCF-7 cells; (A) MCF-7 cells were treated with DMSO, 2.5 µM of **C2**, 2.5 µM of cisplatin independently or in combination for 48 h and cell viability was determined by MTT assay. (B) MCF-7 cells were treated with DMSO, 2.5 µM of **C2**, 2.5 µM of cisplatin independently or in combination for 48 h and cell viability was determined by crystal violet assay.

*2.2.10. **C2** suppresses NOTCH1 dependent signaling pathway*

NOTCH1 signaling pathway plays important role in cancer cells proliferation, invasion and migration. Activation of NOTCH1 signaling promotes tumor growth, development and metastasis. Moreover, NOTCH1 signaling also activates several oncogenic signaling pathways those play critical roles in cancer cell survival. Therefore, inhibition of NOTCH1 signaling is considered important and reduce tumor metastasis, invasion, migration to induce apoptosis of cancer cells. Therefore, we investigated the mechanism aspects of **C2** to suppress cancer cells growth, invasion and migration. Interestingly, **C2** suppressed the expression of NOTCH1 dependent signaling pathway that is important in cancer progression and tumorigenesis (Figure 14A-D). Thus, inhibition of NOTCH1 signaling pathway by **C2** represented the potential and novel role of **C2** in cancer therapy by targeting NOTCH1 signaling pathway. These results also highlighted that **C2** is a novel inhibitor of NOTCH1 signaling pathway that could block downstream signaling pathways of NOTCH1 to trigger apoptosis in cancer cells.

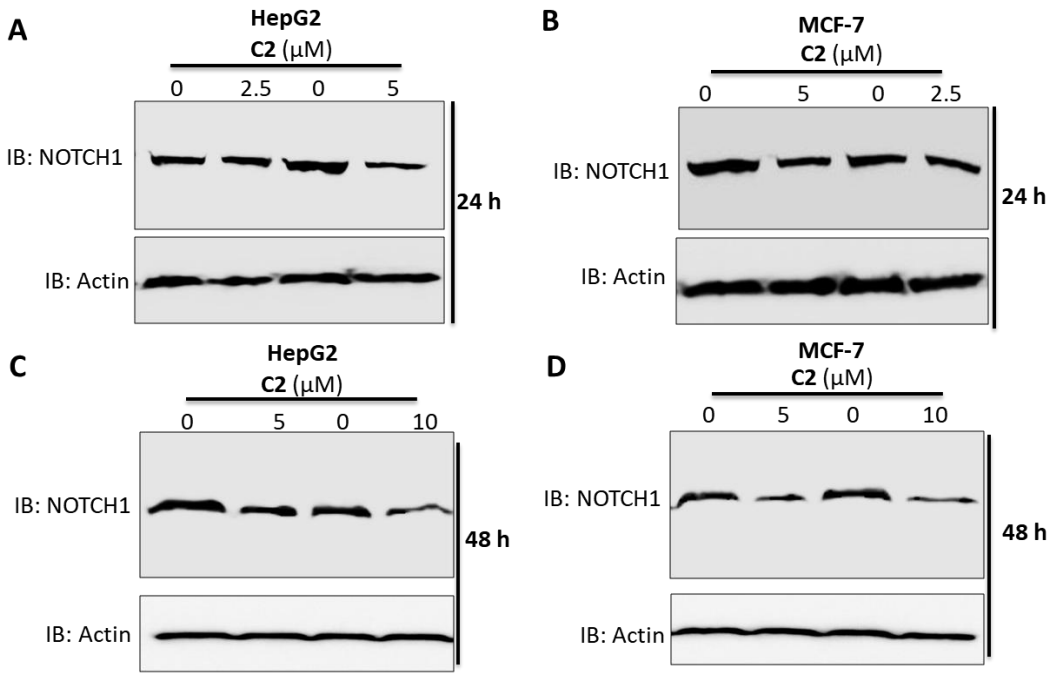

Figure 14. C2 inhibits NOTCH1 dependent signaling pathway; (A and B) HepG2 and MCF-7 cells were treated with DMSO, 2.5 µM or 5 µM of **C2** for 24 h and subjected to western blot to detect NOTCH1 expression. (C and D) HepG2 and MCF-7 cells were treated with DMSO, 5 µM or 10 µM of **C2** for 48 h and subjected to western blot to detect NOTCH1 expression. Actin was used as a loading control in all the experiments.

3. Conclusion

In conclusion, dimetallic ONS-donor ligands derived Ru-(*p*-cymene) mono-cationic complexes were synthesized and characterized by different analytical methods. Three of those complexes were characterized in solid state by single crystal X-ray analysis that described their actual structures and coordination of the ligands. These complexes with functionalized structures confirmed their synthetic feasibility and this slight functional modification on each complex also showed effect on their anticancer effect. The *in vitro* antineoplastic properties of these complexes were investigated in three types of humans cancer cells including breast (MCF-7), lung (A549) and liver (HepG2) cancers. These complexes exerted anticancer effects in multiple human cancer cell lines and showed much better cytotoxic activity as compared to cisplatin or

oxaliplatin. We observed changes in cell morphology and strong effect on wound healing that indicated their anticancer potentials. Consistent with cell migration, we also observed inhibitory effect of these complexes on cell invasion of cancer cells. Suppression of cellular senescence suggested a role in retarding cancer cells growth to suppress cell proliferation, migration and invasion. Cancer cell stemness study results showed their ability to suppress tumor spheroid formation that is correlated with chemoresistance mechanisms thus playing an important role in sensitivity of cancer cells by suppressing the formation of cancer stem cells. More importantly, we observed synergistic anticancer effect of **C2** in combination with cisplatin or natural agents such as vitamin C that points towards the importance of these complexes with other anticancer agents or natural agents. Ultimately searching for novel and potential anticancer mechanisms we observed that these complexes suppressed NOTCH1 oncogenic signaling pathway which play a key role in cancer progression, tumor development, cell migration, invasion and chemoresistance. Taken together, our results highlighted the importance of these Ru(II) complexes in cancer cell death and these complexes may find applications in the field of cancer therapy or anticancer drug development.

4. Materials and Methods

4.1. Chemistry

4.1.1. General experimental

All analytical grade solvents and reagents purchased from commercial sources were used without further purification. Dichloro(*p*-cymene)ruthenium(II) dimer precursor was purchased from J&K Chemicals Shanghai China. ^{1}H and ^{13}C NMR analyses were conducted on a Bruker AVANCE III HD 500 MHz spectrophotometer. HR-ESI-MS analyses were performed using

waters G2-Xs QTof mass spectrometer. Crystal data for **C1**, **C2** and **C4** was collected using our previously reported conditions and structure was solved accordingly [84]. Crystallographic data for each complex can be obtained free of charge from Cambridge Crystallographic Data Center using the number CCDC 2193180 (**C1**), CCDC 2193181 (**C2**) and CCDC 2193182 (**C4**) or through e-mail: deposit@ccdc.cam.ac.uk.

*4.1.2. Synthesis of the ligands (**L1**-**L4**)*

166 mg, 1 mmol of 2,5-dihydroxyterephthalaldehyde was suspended in 15 mL of absolute ethanol in a 50 mL round bottom flask with a magnetic stirrer bar. 2.2 equivalents of the particular amine were dissolved in 5 mL of ethanol and added to the flask in one portion. The mixture was stirred at reflux temperature till completion (checked by TLC). After completion the mixture was cooled in refrigerator overnight, the solid precipitate (in case of **L1**-**L3**) was filtered, washed further with copious amount of cold ethanol and dried under high vacuum. For **L4** after completion of the reaction the mixture was evaporated and a gummy solid was obtained, that was recrystallized form *n*-hexane in refrigerator. Each ligand was obtained in excellent yield with enough purity, the structure details are given while the original data figures were given in the electronic supporting information (ESI) (Figures S1-S31).

L1(2,5-bis(((2-(methylthio)phenyl)imino)methyl)benzene-1,4-diol): Yield 80%, orange solid, FT-IR (KBr Pellet) cm^{-1}: 3440, 2929, 2892,1624, 1455, 1317, 1088, 863, 751, 664, 552. ^{1}H NMR (500 MHz, Chloroform-*d*) δ 12.53 (s, 2H), 8.67 (s, 2H), 7.37 – 7.30 (m, 4H), 7.27 – 7.23 (m, 4H), 7.13 (s, 2H), 2.52 (s, 6H) ppm. ^{13}C NMR (125 MHz, CF_3COOD) δ 155.6, 148.8, 130.5, 129.5, 129.0, 128.9, 125.2, 119.2, 117.3, 114.1, 12.8 ppm. HRMS (ESI): Calcd for $C_{22}H_{21}N_2O_2S_2$: 409.104 for $[M+H]^+$, Found: 409.1043.

L2(2,5-bis(((2-(isopropylthio)phenyl)imino)methyl)benzene-1,4-diol): Yield 86%, orange solid, FT-IR (KBr Pellet) cm^{-1}: 3427, 2921, 1619, 1438, 1373, 1304, 1079, 876, 846, 763, 656, 535. ^{1}H NMR (500 MHz, Chloroform-*d*) δ 12.66 (s, 2H), 8.61 (s, 2H), 7.47 (dd, J = 7.3, 1.9 Hz, 2H), 7.29 (qd, J = 6.9, 1.9 Hz, 4H), 7.26 – 7.23 (m, 2H), 7.10 (s, 2H), 3.44 (hept, J = 6.7 Hz, 2H), 1.35 (d, J = 6.7 Hz, 12H) ppm. ^{13}C NMR (125 MHz, Chloroform-*d*) δ 160.99, 153.04, 147.48, 132.58, 130.90, 127.74, 127.15, 122.72, 119.40, 117.91, 37.14, 23.06 ppm. HRMS (ESI): Calcd for $C_{26}H_{29}N_2O_2S_2$: 465.167 $[M+H]^+$, Found: 465.1669.

L3(2,5-bis(((2-(phenylthio)phenyl)imino)methyl)benzene-1,4-diol): Yield 81%, orange solid, FT-IR (KBr Pellet) cm^{-1}: 3446, 2939, 1629, 1451, 1317, 1135, 1075, 855, 755, 677. ^{1}H NMR (500 MHz, Chloroform-*d*) δ 12.38 (s, 2H), 8.56 (s, 2H), 7.42 (d, J = 7.3 Hz, 4H), 7.39 – 7.27 (m, 10H), 7.18 (d, J = 7.2 Hz, 2H), 7.12 (d, J = 7.8 Hz, 2H), 7.04 (s, 2H) ppm. ^{13}C NMR (125 MHz, CF_3COOD) δ 156.6, 148.9, 132.3, 131.7, 129.0, 128.2, 126.7, 126.0, 125.0, 124.7, 123.5, 119.3, 117.2, 114.8 ppm. HRMS (ESI): Calcd for $C_{32}H_{24}N_2O_2S_2$: 533.136 $[M+H]^+$, Found: 533.1356

L4(2,5-bis(((3-(methylthio)propyl)imino)methyl)benzene-1,4-diol): Yield 65%, yellow shiny crystalline solid, FT-IR (KBr Pellet) cm^{-1}: 3445, 2912, 1633, 1520, 1430, 1334, 1148, 1075, 967, 825, 673, 526. ^{1}H NMR (500 MHz, Chloroform-*d*) δ 12.62 (s, 2H), 8.33 (s, 2H), 6.86 (s, 2H), 3.72 (td, J = 6.6, 1.3 Hz, 4H), 2.59 (t, J = 7.1 Hz, 4H), 2.11 (s, 6H), 2.01 (p, J = 6.9 Hz, 4H) ppm. ^{13}C NMR (125 MHz, $CDCl_3$) δ 164.85, 152.73, 121.30, 118.17, 58.39, 31.71, 29.80, 15.52 ppm. HRMS (ESI): Calcd for $C_{16}H_{25}N_2O_2S_2$: 341.136 $[M+H]^+$, Found: 341.136.

*4.1.3. Procedure for the synthesis of **C1-C4***

1 equivalent 0.1 mmol of the corresponding ligand (**L1-L4)**, 2.2 equivalents. 0.12 mmol of dichloro(*p*-cymene)ruthenium(II) dimer and 2.2 equivalents, 0.22 mmol of sodium acetate were weighed together and added to a 50 mL round bottom flask containing 30 mL of 1:1

mixture of methanol and dichloromethane. The flask was fitted with a condenser and immersed into an oil bath preheated at 50 °C. The mixture was stirred at this temperature until all the ligand was consumed (checked by TLC 10% ethyl acetate/*n*-hexane). After completion the mixture was vacuum evaporated to about 2-4 mL volume. The mixture was added with 20 mL deionized water and excess 4 mmol (4 equivalents) of solid potassium hexafluorophosphate. It was stirred for 30 minutes at rt that precipitated a green solid and the water portion was almost colorless. The solid was filtered and washed with deionized water. Each complex (**C1**-**C4**) was obtained in excellent isolated yield as a green solid.

C1(2,5-bis(((3-(methylthio)propyl)imino)methyl)phenoxy)diruthenium(*p*-cymene)dihexafluorophosphate): Yield 82%, green solid, FT-IR (KBr Pellet) cm^{-1}: 3435, 2947, 2354, 1611, 1433, 1309, 1227, 1118, 1075, 976, 850, 768, 677, 543. ^{1}H NMR (500 MHz, DMSO-d_6) δ 8.58 (s, 1H), 8.46 (s, 1H), 8.01 (s, 2H), 7.90 (s, 2H), 7.66 (s, 2H), 7.48 (d, J = 8.5 Hz, 2H), 7.10 (d, J = 6.4 Hz, 2H), 5.91 (s, 2H), 5.85 (s, 1H), 5.75 (s, 3H), 5.66 (s, 1H), 5.49 (s, 1H), 2.45 – 2.35 (m, 2H), 2.04 (d, J = 33.7 Hz, 6H), 1.92 (s, 3H), 1.71 (s, 3H), 1.04 (d, J = 41.7 Hz, 9H), 0.93 (s, 3H) ppm. Anal. found (calculated for $C_{42}H_{46}N_2O_2Ru_2S_2P_2F_{12}$): C, 43.13 (43.23); H, 4.10 (3.97); N, 2.37 (2.40). HRMS (ESI): Calcd for $[C_{42}H_{46}N_2O_2Ru_2S_2]^{2+}$: $[M\text{-}2PF_6]^{2+}$ 439.054, Found: 439.0515.

C2(2,5-bis(((3-(isopropylthio)propyl)imino)methyl)phenoxy)diruthenium(*p*-cymene)dihexafluorophosphate): Yield 87%, green solid, FT-IR (KBr Pellet) cm^{-1}: 3240, 2947, 1585, 1438, 1313, 1227, 1135, 1062, 842, 673, 552. ^{1}H NMR (500 MHz, DMSO-d_6) δ 8.57 (s, 1H), 8.48 (s, 1H), 8.04 (t, J = 9.2 Hz, 2H), 7.82 (d, J = 7.7 Hz, 2H), 7.69 (t, J = 7.7 Hz, 2H), 7.48 (t, J = 7.4 Hz, 2H), 7.11 (d, J = 3.7 Hz, 2H), 5.99 (d, J = 5.9 Hz, 1H), 5.95 (d, J = 6.0 Hz, 1H), 5.87 (dd, J = 11.8, 6.1 Hz, 2H), 5.76 (d, J = 6.1 Hz, 1H), 5.62 (t, J = 6.7 Hz, 2H), 5.43 (d, J = 6.0

Hz, 1H), 3.16 – 2.90 (m, 2H), 1.86 (s, 3H), 1.69 (s, 3H), 1.22 (d, J = 6.5 Hz, 3H), 1.10 (ddd, J = 20.7, 16.6, 8.6 Hz, 19H), 0.98 (d, J = 6.9 Hz, 3H) ppm. Anal. found (calculated for $C_{46}H_{54}N_2O_2Ru_2S_2P_2F_{12}$): C, 45.08 (45.17); H, 4.58 (4.45); N, 2.3 (2.29). HRMS (ESI): Calcd for $[C_{46}H_{54}N_2O_2Ru_2S_2]^{2+}$: $[M\text{-}2PF_6]^{2+}$ 467.085, Found: 467.0858.

C3(2,5-bis(((3-(phenylylthio)propyl)imino)methyl)phenoxy)diruthenium(*p*-cymene)dihexafluorophosphate): Yield 85%, green solid, FT-IR (KBr Pellet) cm^{-1}: 3440, 2943, 1581, 1438, 1313, 1222, 1123, 846, 755, 673, 556. ^{1}H NMR (500 MHz, DMSO-d_6) δ 8.45 (s, 2H), 7.94 (s, 2H), 7.72 (d, J = 30.8 Hz, 4H), 7.51 (t, J = 7.8 Hz, 2H), 7.34 (s, 6H), 7.17 (s, 4H), 6.92 (s, 2H), 5.86 (d, J = 57.7 Hz, 6H), 5.44 (d, J = 19.9 Hz, 2H), 1.87 – 1.77 (m, 6H), 1.04 (s, 12H) ppm. Anal. found (calculated for $C_{52}H_{50}N_2O_2Ru_2S_2P_2F_{12}$): C, 48.50 (48.37); H, 4.12 (3.9); N, 2.09 (2.17). HRMS (ESI): Calcd for $[C_{52}H_{50}N_2O_2Ru_2S_2]^{2+}$: $[M\text{-}2PF_6]^{2+}$ 501.0695, Found: 501.0701.

C4(2,5-bis(((3-(methylthio)propyl)imino)methyl)phenoxy)diruthenium(*p*-cymene)dihexafluorophosphate): Yield 77%, greenish black solid, FT-IR (KBr Pellet) cm^{-1}: 3435, 2943, 1619, 1438, 1235, 1144, 1049, 846, 673, 560. ^{1}H NMR (500 MHz, DMSO-d_6) δ 8.16 (s, 2H), 6.71 (s, 2H), 5.87 (d, J = 6.1 Hz, 1H), 5.76 (d, J = 6.2 Hz, 3H), 5.67 (d, J = 6.1 Hz, 1H), 5.61 (d, J = 5.9 Hz, 1H), 5.55 (d, J = 6.4 Hz, 2H), 4.26 – 4.13 (m, 2H), 3.90 (t, J = 11.4 Hz, 2H), 3.19 (d, J = 13.7 Hz, 2H), 2.99 (d, J = 12.6 Hz, 2H), 2.63 (q, J = 7.3 Hz, 2H), 2.21 (d, J = 15.1 Hz, 2H), 2.16 (s, 4H), 2.09 (s, 2H), 1.69 (t, J = 14.0 Hz, 2H), 1.52 (s, 2H), 1.46 (s, 4H), 1.15 (d, J = 6.9 Hz, 5H), 1.08 (d, J = 6.8 Hz, 6H), 1.01 (d, J = 6.9 Hz, 2H) ppm. Anal. found (calculated for $C_{36}H_{50}N_2O_2Ru_2S_2\ P_2F_{12}$): C, 53.30 (53.44); H, 6.35 (6.23); N, 3.32 (3.46). HRMS (ESI): Calcd for $[C_{36}H_{50}N_2O_2Ru_2S_2]^{2+}$: $[M\text{-}2PF_6]^{2+}$ 405.0698, Found: 405.0695.

4.2. Biological assays

4.2.1. Cell culture

A549, MCF-7 or HepG2 cells were grown as described previously [84]. Briefly, human lung cancer (A549), human breast cancer (MCF-7) and human liver cancer (HepG2) cells were maintained in DMEM that was supplemented with 10% fetal bovine serum (FBS) and 1% PEST was used as antibiotics. All the cancer cells were grown in CO_2 humidifier at 37 °C. Media was chnaged every third day and all these cells were mainitned in healthy condition.

4.2.2. MTT assay

Cancer cells were plated in 96 well plate and then treated with different doses of the indicated compounds for 24 or 48 h and cell viability was determined by MTT assay as described in our previous report [84]. MTT reagent was added to each 96 well and then cells were incubated for 2 h at 37 °C in an incubator. Finally, media was removed and 100 µL of DMSO was added to each well to dissolve the formazen crystal and aborbance was recored to complete the readaing procedure.

4.2.3. Crystal violet assay

Cancer cells were plated in 24 well plates and then treated with different doses of indicated compounds for 24 and 48 h and cell viability was determined by crystal violet assay. Cells were fixed with acetic acid and methanol mixture for 20 minutes at room temperature and then stained with 0.5% crystal violet for 15 minutes at room temperature. Excess staining was washed out with water and plates were dried and scanned.

4.2.4. Cell morphology detection

Cancer cells were treated with different doses of **C2** for 48 h and cell morphology was detected under microscope using bright field.

4.2.5. Western blots data

MCF-7 or HepG2 cells were treated with DMSO, 2.5 µM and 5 µM of **C2** for 24 or 48 h and subjected to western blot to detect NOTCH1 expression. Briefly, after treatment indicated time point's cell pellets were collected. RIPA lysis buffer was used for cell lysis for 30 minutes on ice box. Cell lysis were quantified and western blot was performed as described previously [84]. NOTCH1 antibody was used to detect NOTCH1 protein.

4.2.6. Tumor spheroids formation assay

Human lung A549, MCF-7 and HepG2 cells were grown in ultra low attachment plates for 5 days as tumor spheroids. 24 h after plating the cells were treated with **C2** and DMSO for 5 days and were grown as tumor spheroids. Mammosphere assay reagents were used for tumor spheroids assay as described previously [84].

4.2.7. Invasion assay

Cancer cells invasion assay was performed as we described previously [84] briefly, A549, MCF-7 or HepG2 cells were treated with 5 μM of **C2** for 24 h and then subjected to invasion assay.

4.2.8. Wound healing assay

HepG2, A549 or MCF7 human cancer cells were plated in 12 well plates at a confluence of 80- 90% and then next day scratch was performed in each well treated with DMSO or **C2**. After 24 h wound healing area was determined under microscope.

Acknowledgements

The authors acknowledge the Inner Mongolia University funding under the title Academic Backbone (No. 10000–21311201/092), Inner Mongolia Autonomous Region Funding No. 21300-5213122, Science and Technology Major Project of Inner Mongolia Autonomous Region No. 2020ZD15, funding from the Science & Technology Department of Inner Mongolia Autonomous Region (No. 2021CG0029, No. 21300-5213402 or No. 15000021T000000020229), and “JUN-MA” High-level Talents Program of Inner Mongolia University (No. 21300–5195112, No. 21300–5205107).

Appendix A. Supplementary data

Supplementary data ^{1}H, ^{13}C NMR spectra, ESI-MS spectrogram related to this article can be found at http://dx.doi.org/10.

References

[1] A.G. Clark, D.M. Vignjevic, Modes of cancer cell invasion and the role of the microenvironment, Curr. Opin. Cell Biol., 36(2015) 13-22.

[2] P. Friedl, K. Wolf, Tumour-cell invasion and migration: Diversity and escape mechanisms, Nat. Rev. Cancer, 3(2003) 362-74.

[3] S. Vinogradov, X. Wei, Cancer stem cells and drug resistance: The potential of nanomedicine, Nanomedicine (Lond), 7(2012) 597-615.

[4] Y. Li, Z. Wang, J.A. Ajani, S. Song, Drug resistance and cancer stem cells, Cell Commun. Signal., 19(2021) 19.

[5] X. Yuan, H. Wu, H. Xu, H. Xiong, Q. Chu, S. Yu, G.S. Wu, K. Wu, Notch signaling: An emerging therapeutic target for cancer treatment, Cancer Lett., 369(2015) 20-7.

[6] L. Gharaibeh, N. Elmadany, K. Alwosaibai, W. Alshaer, Notch1 in cancer therapy: Possible clinical implications and challenges, Mol. Pharmacol., 98(2020) 559-76.

[7] A. Tyagi, A.K. Sharma, C. Damodaran, A review on notch signaling and colorectal cancer, Cells, 9(2020).

[8] D. Anusewicz, M. Orzechowska, A.K. Bednarek, Notch signaling pathway in cancer-review with bioinformatic analysis, Cancers (Basel), 13(2021).

[9] C. Sonkar, S. Sarkar, S. Mukhopadhyay, Ruthenium(ii)-arene complexes as anti-metastatic agents, and related techniques, RSC Med Chem, 13(2022) 22-38.

[10] S.T. Pan, Z.L. Li, Z.X. He, J.X. Qiu, S.F. Zhou, Molecular mechanisms for tumour resistance to chemotherapy, Clin. Exp. Pharmacol. Physiol., 43(2016) 723-37.

[11] L. Galluzzi, L. Senovilla, I. Vitale, J. Michels, I. Martins, O. Kepp, M. Castedo, G. Kroemer, Molecular mechanisms of cisplatin resistance, Oncogene, 31(2012) 1869-83.

[12] D.W. Shen, L.M. Pouliot, M.D. Hall, M.M. Gottesman, Cisplatin resistance: A cellular self-defense mechanism resulting from multiple epigenetic and genetic changes, Pharmacol. Rev., 64(2012) 706-21.

[13] B. Rosenberg, L. Vancamp, T. Krigas, Inhibition of cell division in *Escherichia Coli* by electrolysis products from a platinum electrode, Nature, 205(1965) 698-9.

[14] B. Rosenberg, L. Vancamp, J.E. Trosko, V.H. Mansour, Platinum compounds - A new class of potent antitumour agents, Nature, 222(1969) 385-6.

[15] B. Lippert, Cisplatin: Chemistry and biochemistry of a leading anticancer drug: Verlag Helvetica Chimica Acta Zurich, Swithzerland; 1999.

[16] B. Rosenberg, L. Vancamp, E.B. Grimley, A.J. Thomson, Inhibition of growth or cell division in *Escherichia Coli* by different ionic species of platinu(IV) complexes, J. Biol. Chem., 242(1967) 1347-52.

[17] J.R. García-Berrocal, J. Nevado, R. Ramírez-Camacho, R. Sanz, J.A. González-García, C. Sánchez-Rodríguez, B. Cantos, P. España, J.M. Verdaguer, A. Trinidad Cabezas, The anticancer drug cisplatin induces an intrinsic apoptotic pathway inside the inner ear, Br. J. Pharmacol., 152(2007) 1012-20.

[18] R.S.A. J A Levi, D N Dalley, Haemolytic anemia after cisplatin, Br. Med. J., 282(1981) 2003–4.

[19] R.E. Windsor, S.J. Strauss, C. Kallis, N.E. Wood, J.S. Whelan, Germline genetic polymorphisms may influence chemotherapy response and disease outcome in osteosarcoma, Cancer, 118(2012) 1856-67.

[20] O.D. Castelán-Martínez, R. Jiménez-Méndez, F. Rodríguez-Islas, M. Fierro-Evans, B.E. Vázquez-Gómez, A. Medina-Sansón, P. Clark, B. Carleton, C. Ross, C. Hildebrand, G. Castañeda-Hernández, R. Rivas-Ruiz, Hearing loss in Mexican children treated with cisplatin, Int. J. Pediatr. Otorhi., 78(2014) 1456-60.

[21] R.P. Miller, R.K. Tadagavadi, G. Ramesh, W.B. Reeves, Mechanisms of cisplatin nephrotoxicity, Toxins (Basel), 2(2010) 2490-518.

[22] I. Potocnjak, I. Gobin, R. Domitrovic, Carvacrol induces cytotoxicity in human cervical cancer cells but causes cisplatin resistance: Involvement of MEK-ERK activation, Phytother. Res., (2018) 1-8.

[23] L. Kelland, The resurgence of platinum-based cancer chemotherapy, Nat. Rev. Cancer, 7(2007) 573-84.

[24] N.J. Wheate, S. Walker, G.E. Craig, R. Oun, The status of platinum anticancer drugs in the clinic and in clinical trials, Dalton. Trans., 39(2010) 8113-27.

[25] H.H.A.-S.d. Adnan Salim Abu-Surrah, Maher Y. Abdalla, Palladium-based chemotherapeutic agents: Routes toward complexes with good antitumor activity, Cancer Therapy, 6(2008) 1-10.

[26] E. Ulukaya, F.M. Frame, B. Cevatemre, D. Pellacani, H. Walker, V.M. Mann, M.S. Simms, M.J. Stower, V.T. Yilmaz, N.J. Maitland, Differential cytotoxic activity of a novel palladium-

based compound on prostate cell lines, primary prostate epithelial cells and prostate stem cells, PloS one, 8(2013) e64278.

[27] C. Santini, M. Pellei, V. Gandin, M. Porchia, F. Tisato, C. Marzano, Advances in copper complexes as anticancer agents, Chem. Rev., 114(2013) 815-62.

[28] N. Cutillas, G.S. Yellol, C. de Haro, C. Vicente, V. Rodríguez, J. Ruiz, Anticancer cyclometalated complexes of platinum group metals and gold, Coord. Chem. Rev., 257(2013) 2784-97.

[29] M. Grazul, E. Budzisz, Biological activity of metal ions complexes of chromones, coumarins and flavones, Coord. Chem. Rev., 253(2009) 2588-98.

[30] S.E. Sherman, S.J. Lippard, Structural aspects of platinum anticancer drug interactions with DNA, Chem. Rev., 87(1987) 1153-81.

[31] J. Reedijk, The mechanism of action of platinum anti-tumor drugs, Pure Appl. Chem., 59(1987) 181-92.

[32] Z. Liu, S. Tan, Y. Zu, Y. Fu, R. Meng, Z. Xing, The interactions of cisplatin and DNA studied by atomic force microscopy, Micron, 41(2010) 833-9.

[33] D. Musumeci, C. Platella, C. Riccardi, A. Merlino, T. Marzo, L. Massai, L. Messori, D. Montesarchio, A first-in-class and a fished out anticancer platinum compound: cis-$[PtCl_2(NH_3)_2]$ and cis-$[PtI_2(NH_3)_2]$ compared for their reactivity towards DNA model systems, Dalton. Trans., 45(2016) 8587-600.

[34] M.A. Sgambellone, A. David, R.N. Garner, K.R. Dunbar, C. Turro, Cellular toxicity induced by the photorelease of a caged bioactive molecule: design of a potential dual-action Ru(II) complex, J. Am. Chem. Soc., 135(2013) 11274-82.

[35] J.J. Soldevila-Barreda, I. Romero-Canelon, A. Habtemariam, P.J. Sadler, Transfer hydrogenation catalysis in cells as a new approach to anticancer drug design, Nat. Comm., 6(2015) 1-9.

[36] Z. Xu, S. Swavey, Photoinduced DNA binding of a multi-metallic (Cu(II)/Ru(II)/Pt(II)) porphyrin complex, Inorg. Chem. Commun., 14(2011) 882-3.

[37] C. Acilan, B. Cevatemre, Z. Adiguzel, D. Karakas, E. Ulukaya, N. Ribeiro, I. Correia, J.C. Pessoa, Synthesis, biological characterization and evaluation of molecular mechanisms of novel copper complexes as anticancer agents, Biochim. Biophys. Acta, 1861(2017) 218-34.

[38] K. Suntharalingam, D.J. Hunt, A.A. Duarte, A.J. White, D.J. Mann, R. Vilar, A tri-copper(II) complex displaying DNA-cleaving properties and antiproliferative activity against cancer cells, Chem. Eur. J., 18(2012) 15133-41.

[39] C.R. Munteanu, K. Suntharalingam, Advances in cobalt complexes as anticancer agents, Dalton. Trans., 44(2015) 13796-808.

[40] S.B. Chanu, S. Banerjee, M. Roy, Potent anticancer activity of photo-activated oxo-bridged diiron(III) complexes, Eur. J. Med. Chem., 125(2016) 816-24.

[41] J. Fernandez-Gallardo, B.T. Elie, T. Sadhukha, S. Prabha, M. Sanau, S.A. Rotenberg, J.W. Ramos, M. Contel, Heterometallic titanium-gold complexes inhibit renal cancer cells in vitro and in vivo, Chem. Sci., 6(2015) 5269-83.

[42] T. Lazarevic, A. Rilak, Z.D. Bugarcic, Platinum, palladium, gold and ruthenium complexes as anticancer agents: Current clinical uses, cytotoxicity studies and future perspectives, Eur. J. Med. Chem., 142(2017) 8-31.

[43] A. Petit, F. Mwale, D.J. Zukor, I. Catelas, J. Antoniou, O.L. Huk, Effect of cobalt and chromium ions on bcl-2, bax, caspase-3, and caspase-8 expression in human U937 macrophages, Biomaterials, 25(2004) 2013-8.

[44] S. Bhattacharyya, A. Sarkar, S.K. Dey, A. Mukherjee, Effect of glucosamine conjugation to zinc(II) complexes of a bis-pyrazole ligand: syntheses, characterization and anticancer activity, J. Inorg. Biochem., 140(2014) 131-42.

[45] V. Pierroz, T. Joshi, A. Leonidova, C. Mari, J. Schur, I. Ott, L. Spiccia, S. Ferrari, G. Gasser, Molecular and cellular characterization of the biological effects of ruthenium(II) complexes incorporating 2-pyridyl-2-pyrimidine-4-carboxylic acid, J. Am. Chem. Soc., 134(2012) 20376-87.

[46] A. Frei, R. Rubbiani, S. Tubafard, O. Blacque, P. Anstaett, A. Felgentrager, T. Maisch, L. Spiccia, G. Gasser, Synthesis, characterization, and biological evaluation of new Ru(II) polypyridyl photosensitizers for photodynamic therapy, J. Med. Chem., 57(2014) 7280-92.

[47] H. Huang, B. Yu, P. Zhang, J. Huang, Y. Chen, G. Gasser, L. Ji, H. Chao, Highly charged ruthenium(II) polypyridyl complexes as lysosome-localized photosensitizers for two-photon photodynamic therapy, Angew. Chem., 127(2015) 14255-8.

[48] R. Padilla, J.A. Rodriguez-Corrales, L.E. Donohoe, B.S. Winkel, K.J. Brewer, A new class of Ru(II) polyazine agents with potential for photodynamic therapy, Chem. Commun. (Camb), 52(2016) 2705-8.

[49] G. Suss-Fink, Arene ruthenium complexes as anticancer agents, Dalton. Trans., 39(2010) 1673-88.

[50] P.J. Dyson, Systematic design of a targeted organometallic antitumour drug in pre-clinical development, CHIMIA, 61(2007) 698.

[51] Z.F. Chen, Q.P. Qin, J.L. Qin, J. Zhou, Y.L. Li, N. Li, Y.C. Liu, H. Liang, Water-soluble ruthenium(II) complexes with chiral 4-(2,3-dihydroxypropyl)-formamide oxoaporphine (FOA): In vitro and in vivo anticancer activity by stabilization of G-quadruplex DNA, inhibition of telomerase activity, and induction of tumor cell apoptosis, J. Med. Chem., 58(2015) 4771-89.

[52] K.J. Kilpin, P.J. Dyson, Enzyme inhibition by metal complexes: concepts, strategies and applications, Chem. Sci., 4(2013) 1410-9.

[53] H. Huang, P. Zhang, B. Yu, Y. Chen, J. Wang, L. Ji, H. Chao, Targeting nucleus DNA with a cyclometalated dipyridophenazineruthenium(II) complex, J. Med. Chem., 57(2014) 8971-83.

[54] A. Grozav, O. Balacescu, L. Balacescu, T. Cheminel, I. Berindan-Neagoe, B. Therrien, Synthesis, anticancer activity, and genome profiling of thiazolo arene ruthenium complexes, J. Med. Chem., 58(2015) 8475-90.

[55] A. Bergamo, A. Masi, A.F. Peacock, A. Habtemariam, P.J. Sadler, G. Sava, In vivo tumour and metastasis reduction and in vitro effects on invasion assays of the ruthenium RM175 and osmium AFAP51 organometallics in the mammary cancer model, J. Inorg. Biochem., 104(2010) 79-86.

[56] P. Zhang, P.J. Sadler, Redox-active metal complexes for anticancer therapy, Eur. J. Inorg. Chem., 2017(2017) 1541-8.

[57] Q. Sun, Y. Li, H. Shi, Y. Wang, J. Zhang, Q. Zhang, Ruthenium complexes as promising candidates against lung cancer, Molecules, 26(2021).

[58] S.M. Meier, M. Novak, W. Kandioller, M.A. Jakupec, V.B. Arion, N. Metzler-Nolte, B.K. Keppler, C.G. Hartinger, Identification of the structural determinants for anticancer activity of a ruthenium arene peptide conjugate, Chem. Eur. J., 19(2013) 9297-307.

[59] Z. Wang, H. Qian, S.M. Yiu, J. Sun, G. Zhu, Multi-targeted organometallic ruthenium(II)-arene anticancer complexes bearing inhibitors of poly(ADP-ribose) polymerase-1: A strategy to improve cytotoxicity, J. Inorg. Biochem., 131(2014) 47-55.

[60] W. Su, Z. Tang, P. Li, Development of arene ruthenium antitumor complexes, Mini-Rev. Med. Chem., 16(2016) 787-95.

[61] M.J. Chow, C. Licona, D. Yuan Qiang Wong, G. Pastorin, C. Gaiddon, W.H. Ang, Discovery and investigation of anticancer ruthenium-arene Schiff-base complexes via water-promoted combinatorial three-component assembly, J. Med. Chem., 57(2014) 6043-59.

[62] S.J. Dougan, A. Habtemariam, S.E. McHale, S. Parsons, P.J. Sadler, Catalytic organometallic anticancer complexes, Proc. Natl. Acad. Sci. U. S. A., 105(2008) 11628-33.

[63] C.M. Clavel, E. Păunescu, P. Nowak-Sliwinska, A.W. Griffioen, R. Scopelliti, P.J. Dyson, Modulating the anticancer activity of ruthenium(II)–arene complexes, J. Med. Chem., 58(2015) 3356-65.

[64] G.R. Jadhav, S. Sinha, M. Chhabra, P. Paira, Synthesis of novel anticancer ruthenium–arene pyridinylmethylene scaffolds via three-component reaction, Bioorg. Med. Chem. Lett., 26(2016) 2695-700.

[65] L. Zeng, P. Gupta, Y. Chen, E. Wang, L. Ji, H. Chao, Z.-S. Chen, The development of anticancer ruthenium(ii) complexes: from single molecule compounds to nanomaterials, Chem. Soc. Rev., 46(2017) 5771-804.

[66] C.G.L. Nongpiur, A.K. Verma, R.K. Singh, M.M. Ghate, K.M. Poluri, W. Kaminsky, M.R. Kollipara, Half-sandwich ruthenium(II), rhodium(III) and iridium(III) fluorescent metal

complexes containing pyrazoline based ligands: DNA binding, cytotoxicity and antibacterial activities, J. Inorg. Biochem., 238(2023) 112059.

[67] M. Silva, R. Vinck, Y. Wang, B. Saubamea, M. Tharaud, E. Dominguez-Jurado, J. Karges, P.M.P. Gois, G. Gasser, Towards selective delivery of a ruthenium(II) polypyridyl complex-containing bombesin conjugate into cancer cells, ChemBioChem, 24(2023) e202200647.

[68] C. Sumithaa, M. Ganeshpandian, Half-sandwich ruthenium arene complexes bearing clinically approved drugs as ligands: The importance of metal-drug synergism in metallodrug design, Mol. Pharm., 20(2023) 1453-79.

[69] C. Sumithaa, T. Manjunathan, O. Mazuryk, S. Peters, R.S. Pillai, M. Brindell, P. Gopinath, M. Ganeshpandian, Nanoencapsulation of Ru(p-cymene) complex bearing ginger-based natural product into liposomal nanoformulation to improve Its cellular uptake and antiproliferative activity, ACS Appl Bio Mater, 5(2022) 3241-56.

[70] Y. Lu, D. Zhu, Q. Le, Y. Wang, W. Wang, Ruthenium-based antitumor drugs and delivery systems from monotherapy to combination therapy, Nanoscale, 14(2022) 16339-75.

[71] L. Conti, E. Macedi, C. Giorgi, B. Valtancoli, V. Fusi, Combination of light and Ru(II) polypyridyl complexes: Recent advances in the development of new anticancer drugs, Coord. Chem. Rev., 469(2022).

[72] A. Gandioso, K. Purkait, G. Gasser, Recent approaches towards the development of ru(II) polypyridyl complexes for anticancer photodynamic therapy, Chimia (Aarau), 75(2021) 845-55.

[73] C. Zhang, T. Kang, X. Wang, J. Song, J. Zhang, G. Li, Stimuli-responsive platinum and ruthenium complexes for lung cancer therapy, Front Pharmacol, 13(2022) 1035217.

[74] R. Pettinari, F. Marchetti, F. Condello, C. Pettinari, G. Lupidi, R. Scopelliti, S. Mukhopadhyay, T. Riedel, P.J. Dyson, Ruthenium(II)–arene RAPTA type complexes containing curcumin and bisdemethoxycurcumin display potent and selective anticancer activity, Organometallics, 33(2014) 3709-15.

[75] W.-G. Jia, H. Zhang, T. Zhang, S. Ling, Synthesis, structures and catalytic activities of half-sandwich ruthenium complexes based on Schiff Base ligands, Inorg. Chem. Commun., 66(2016) 15-8.

[76] H.S. Çalık, E. Ispir, Ş. Karabuga, M. Aslantas, Ruthenium (II) complexes of NO ligands: Synthesis, characterization and application in transfer hydrogenation of carbonyl compounds, J. Organomet. Chem., 801(2016) 122-9.

[77] R. Raveendran, S. Pal, Ruthenium(II) complexes with 2-(benzylimino-methyl)-4-R-phenol containing the *trans*(PPh_3), *cis*(CO, Cl)-$\{Ru(PPh_3)_2(CO)Cl\}^+$ unit, J. Organomet. Chem., 695(2010) 630-3.

[78] M.G. Mendoza-Ferri, C.G. Hartinger, M.A. Mendoza, M. Groessl, A.E. Egger, R.E. Eichinger, J.B. Mangrum, N.P. Farrell, M. Maruszak, P.J. Bednarski, F. Klein, M.A. Jakupec, A.A. Nazarov, K. Severin, B.K. Keppler, Transferring the concept of multinuclearity to ruthenium complexes for improvement of anticancer activity, J. Med. Chem., 52(2009) 916-25.

[79] F.-U. Rahman, M.Z. Bhatti, A. Ali, H.-Q. Duong, Y. Zhang, X. Ji, Y. Lin, H. Wang, Z.-T. Li, D.-W. Zhang, Dimetallic Ru(II) arene complexes appended on bis-salicylaldimine induce cancer cell death and suppress invasion via p53-dependent signaling, Eur. J. Med. Chem., 157(2018) 1480-90.

[80] L. Cubo, A. Casini, C. Gabbiani, G. Mastrobuoni, L. Messori, J. Jimenez-Barbero, C. Navarro-Ranninger, A.G. Quiroga, Solution behaviour and biomolecular interactions of two cytotoxic trans-platinum(II) complexes bearing aliphatic amine ligands, Chem. Eur. J., 15(2009) 9139-46.

[81] M. Haghdoost, G. Golbaghi, M. Létourneau, S.A. Patten, A. Castonguay, Lipophilicity-antiproliferative activity relationship study leads to the preparation of a ruthenium(II) arene complex with considerable in vitro cytotoxicity against cancer cells and a lower in vivo toxicity in zebrafish embryos than clinically approved cisplatin, Eur. J. Med. Chem., 132(2017) 282-93.

[82] M.M. Haghdoost, J. Guard, G. Golbaghi, A. Castonguay, Anticancer activity and catalytic potential of ruthenium(II)-arene complexes with N,O-donor ligands, Inorg. Chem., 57(2018) 7558-67.

[83] X. Bai, A. Ali, N. Wang, Z. Liu, Z. Lv, Z. Zhang, X. Zhao, H. Hao, Y. Zhang, F.U. Rahman, Inhibition of SREBP-mediated lipid biosynthesis and activation of multiple anticancer mechanisms by platinum complexes: Ascribe possibilities of new antitumor strategies, Eur. J. Med. Chem., 227(2022) 113920.

[84] X. Bai, A. Ali, Z. Lv, N. Wang, X. Zhao, H. Hao, Y. Zhang, F.-U. Rahman, Platinum complexes inhibit HER-2 enriched and triple-negative breast cancer cells metabolism to suppress growth, stemness and migration by targeting PKM/LDHA and CCND1/BCL2/ATG3 signaling pathways, Eur. J. Med. Chem., 224(2021) 113689.

[85] F.U. Rahman, A. Ali, H.Q. Duong, I.U. Khan, M.Z. Bhatti, Z.T. Li, H. Wang, D.W. Zhang, ONS-donor ligand based Pt(II) complexes display extremely high anticancer potency through autophagic cell death pathway, Eur. J. Med. Chem., 164(2019) 546-61.

[86] M.Z. Bhatti, A. Ali, H.Q. Duong, J. Chen, F.U. Rahman, Anticancer activity and mechanism of bis-pyrimidine based dimetallic Ru(II)-(*p*-cymene) complex in human non-small cell lung cancer via p53-dependent pathway, J. Inorg. Biochem., 194(2019) 52-64.

[87] J. Ming, M.Z. Bhatti, A. Ali, Z. Zhang, N. Wang, A. Mohyuddin, J. Chen, Y. Zhang, F.U. Rahman, Vitamin B_6 based Pt(II) complexes: Biomolecule derived potential cytotoxic agents for thyroid cancer, Metallomics, (2022).

[88] J.E. Kim, J.S. Kang, W.J. Lee, Vitamin C induces apoptosis in human colon cancer cell line, HCT-8 via the modulation of calcium influx in endoplasmic reticulum and the dissociation of bad from 14-3-3beta, Immune Netw., 12(2012) 189-95.

[89] J.Y. Lim, D. Kim, B.R. Kim, J.S. Jun, J.S. Yeom, J.S. Park, J.H. Seo, C.H. Park, H.O. Woo, H.S. Youn, S.C. Baik, W.K. Lee, M.J. Cho, K.H. Rhee, Vitamin C induces apoptosis in AGS cells via production of ROS of mitochondria, Oncol. Lett., 12(2016) 4270-6.

[90] J. Cha, M.W. Roomi, V. Ivanov, T. Kalinovsky, A. Niedzwiecki, M. Rath, Ascorbate supplementation inhibits growth and metastasis of B16FO melanoma and 4T1 breast cancer cells in vitamin C-deficient mice, Int. J. Oncol., 42(2013) 55-64.

[91] L.H. Zeng, Q.M. Wang, L.Y. Feng, Y.D. Ke, Q.Z. Xu, A.Y. Wei, C. Zhang, R.B. Ying, High-dose vitamin C suppresses the invasion and metastasis of breast cancer cells via inhibiting epithelial-mesenchymal transition, Onco. Targets Ther., 12(2019) 7405-13.

[92] G.V. Kondagunta, J. Bacik, A. Donadio, D. Bajorin, S. Marion, J. Sheinfeld, G.J. Bosl, R.J. Motzer, Combination of paclitaxel, ifosfamide, and cisplatin is an effective second-line therapy for patients with relapsed testicular germ cell tumors, J. Clin. Oncol., 23(2005) 6549-55.

[93] I.W. Achkar, N. Abdulrahman, H. Al-Sulaiti, J.M. Joseph, S. Uddin, F. Mraiche, Cisplatin based therapy: the role of the mitogen activated protein kinase signaling pathway, J. Transl. Med., 16(2018) 96.

[94] H. Wu, H. Jin, C. Wang, Z. Zhang, H. Ruan, L. Sun, C. Yang, Y. Li, W. Qin, C. Wang, Synergistic cisplatin/doxorubicin combination chemotherapy for multidrug-resistant cancer via polymeric nanogels targeting delivery, ACS Appl. Mater. Interfaces, 9(2017) 9426-36.